



OCEAN ENGINEERING
TEXAS A&M UNIVERSITY



Port Aransas Ferry – Impacts to Operation Analysis

Final Report

Prepared by

Jens Figlus, Youn-Kyung Song, and Marc Perlin

Department of Ocean Engineering

Texas A&M University

Galveston, TX 77553

Prepared for

Texas Department of Transportation (TXDOT)

Maritime Division



December 2020

(This page was left blank intentionally)

EXECUTIVE SUMMARY

This study addresses the Texas Department of Transportation (TXDOT) Port Aransas Ferry (ferry) system. It assesses the impacts on ferry operations and infrastructure caused by the proposed Corpus Christi Ship Channel (CCSC) deepening projects and the proposed installation of a Very Large Crude Carrier (VLCC) terminal on Harbor Island just east of the northern ferry landing. The impact of VLCCs crossing the ferry route is investigated as well, due to the fact that an additional VLCC terminal is envisioned at a location further west of the ferry terminal toward Corpus Christi Bay. The intent of this report is to provide a high-level assessment of the current and planned projects to identify any potential issues that may require further TXDOT action. In particular, worst-case scenario parameters for the VLCC dimensions and movement were used in combination with empirical equations to assess potential hydrodynamic impacts to ferry operations.

The installation of an additional VLCC terminal west of the ferry landings could cause significant impact to ferry operations due to VLCC vessels crossing the ferry path. VLCC drawdown, wake, and return current parameters in combination with ship channel geometry have the potential to cause temporary unsafe ferry operating conditions and extended scour at landing quay walls. The present study reveals the potential for VLCC-generated hydrodynamics on the order of safe ferry operation limits. Such a future project proposal and its potential impacts would have to be investigated in further detail.

Analysis of available data revealed that the planned channel deepening projects would not have major impacts on ferry operations in the form of changes in currents and wind wave effects. However, the planned installation of a quay wall between the new terminal basin and the northern ferry landing with a potential extension toward the ship channel requires further investigation to avoid negative effects on ferry operations. The quay wall is intended to control modified circulation patterns during peak tidal currents resulting from the construction of the new VLCC terminal basin. Since the installation of the new VLCC terminal on Harbor Island does not require VLCC movement past the ferry landings, the impact of potential drawdown, vessel wake, or propeller wash on ferry operations is deemed not significant. The situation changes if VLCCs cross the ferry path as stated in the previous paragraph.

As several studies related to the Harbor Island project and channel-deepening efforts are still ongoing, it is recommended to continue to take a proactive approach and address potential issues by synthesizing the results of ongoing numerical vessel passing studies from various entities, once available, to further identify and quantify changes in hydrodynamics due to altered CCSC geometry, structural modifications, and VLCC movement. This effort should also include a separate numerical modeling analysis on vessel impacts to ferry operations that can address complexities beyond the present first-order empirical analysis.

TABLE OF CONTENTS

1. INTRODUCTION.....	1
1.1. Background	1
1.2. Proposed Modifications in the Vicinity of the Ferry Terminals	1
1.2.1. Channel Deepening to 54 feet below MLLW	1
1.2.2. VLCC Terminal Installation on Harbor Island	2
1.2.3. Channel Deepening to 79 feet below MLLW near the Ferry.....	4
1.3. Vessels, Facilities, and Operations.....	5
1.3.1. VLCC Specifications	5
1.3.2. Ferry Landing Structures	6
1.3.3. Ferry Vessels	8
1.3.4. Ferry Operations and Regulations	10
2. EXISTING ENVIRONMENTAL CONDITIONS.....	12
2.1. Datums	12
2.2. Coastal Climate	12
2.2.1. Tidal Water-Level Fluctuations.....	13
2.2.2. Winds.....	13
2.2.3. Waves.....	14
2.2.4. Currents.....	15
2.2.5. Precipitation and Temperature	17
2.2.6. Sea Level Trends	17
2.3. Channel Geomorphology and Sediments.....	19
3. IMPACT EVALUATION.....	23
3.1. Hydrodynamics in Navigation Channels	23
3.1.1. Hydrodynamic Impact of Channel Modifications.....	23
3.1.2. Empirical Equations for Deep Draft Vessel Hydrodynamics	23
3.1.3. Propeller Wash	28
3.2. Quantification of Vessel Induced Hydrodynamics.....	32
3.2.1. Assumptions and Limitations.....	32
3.2.2. Waves Produced by VLCC Motion.....	32
3.2.3. Propeller Wash Analysis Results.....	35
3.3. Morphological Changes.....	37
4. FINDINGS AND RECOMMENDATIONS	39
5. ACKNOWLEDGEMENTS	41
6. REFERENCES.....	41
7. Appendix	45

List of Figures

Figure 1-1. Port Aransas ferry study area.....	1
Figure 1-2. Current CCCIP construction layout and project schedule (Port of Corpus Christi Authority, 2018).	2
Figure 1-3. Project site plan for two berth structures of the new VLCC terminal proposed to be constructed in the southern portion of Harbor Island in Nueces County, Texas (Source: Wood Environment & Infrastructure Solutions, Inc., 2019).	3
Figure 1-4. Proposed dredging plan for deepening and extending the portion of the CCSC from Harbor Island into Gulf of Mexico to the maximum 80 feet below MLLW (AECOM, 2019).	4
Figure 1-5. Photo of a VLCC for illustration purposes.	6
Figure 1-6. Planview of Mustang Island landing blueprint excerpt (source: TXDOT).....	7
Figure 1-7. Elevation side view of Harbor Island landing blueprint excerpt showing the front elevation of the bulkhead and cap (source: TXDOT).	8
Figure 1-8: Photo of new 28-car passenger ferry Amadeo Saenz Jr (photo: TXDOT).....	9
Figure 1-9. Schematic of outboard profile (top) and deck planview (bottom) of 28-car ferry type (source: TXDOT).....	10
Figure 2-1. Tidal water levels observed near the ferry system in 2019. The hourly water level time series was obtained from nearby NOAA CO-OPS Station at Port Aransas, TX (8775237).	13
Figure 2-2. Hourly wind observed in the Port Aransas area during 2019. The upper and lower panels show annual time series and statistical distributions, respectively, of speed (a, c) and direction (b, d) of the local wind. Direction indicates where wind is coming from in degrees clockwise from true north.	14
Figure 2-3. Depth-averaged current (U_{95}) during slack to ebb tidal stage in the CCSC between Harbor Island and Port Aransas. (a) Spatial and (b-c) statistical distributions of speed and direction of U_{95} . The direction of U_{95} refers to the current heading measured clockwise from true north. Field current measurements were conducted on September 22, 2019, from 11 AM to 12 PM.....	15
Figure 2-4. Depth-averaged current (U_{95}) during flood to slack tidal stage in the CCSC between Harbor Island and Port Aransas. (a) Spatial and (b-c) statistical distributions of speed and direction of U_{95} . The direction of U_{95} refers to the current heading measured clockwise from true north. Field current measurements were conducted on September 26, 2019, from 3 PM to 5 PM.	16
Figure 2-5. Rainfall amount, air, and water temperature observed near the ferry system. The annual precipitation (a) and air and water temperature (b and c) were obtained from the NOAA CO-OPS Station Port Aransas, TX (8775237).	17
Figure 2-6. Average seasonal cycle of average mean sea levels (a) and RSL (Relative Sea Level) trend (b) estimated for the Corpus Christi Bay area. Monthly mean sea level data between 1983 and 2019 were obtained from the long-term water level station located offshore Corpus Christi Bay (Station #: 8775870). The 95% confidence intervals in the seasonal mean seal level and linear trend in RSL are calculated using a minimum span of 30 years of station tide data averaged over each month.	18
Figure 2-7. Present and planned dredging cross sections for the CCSC in the ferry area. The current bed positions (red, dashed lines) in the study segments generally comply with the existing 54' depth dredge template (gray, dashed lines), whereas the proposed 78' depth plan will implement deeper profiles (thick, solid line). The cross section locations selected for display are denoted in Figure 1-1 and Figure 1-2. (Source: AECOM, 2019).	20
Figure 2-8. Map showing USACE sediment-core sample location 3ST-136.	21

Figure 2-9. Grain size distribution of surface grab sample in the CCSC at the ferry location (source: USACE).	22
Figure 3-1. Deformation of the water surface (top view) induced by a vessel navigating from left to right in a confined channel (BAW, 2011).	24
Figure 3-2. Definition sketch for the channel cross-section with respect to the mean water depth (BAW, 2011).	25
Figure 3-3. Measured water level time series of ship generated waves created by the passenger ferry Baltic Princess. Modified from Figure 1 of Almström et al., (2014).	27
Figure 3-4. Schematic illustration of the parameters used to compute the distribution of near-bed flow velocities orthogonal to the jet axis (BAW, 2005).	31
Figure 3-5. Simplified 79-ft depth (MLLW) profile between the cross-section location EE' and FF' shown in Figure 1-1. The bottom width varied from 530 to 615 ft along the channel distance $l = 8,000$ ft.	33
Figure 3-6. Maximum main velocity, $v_{x,max}$, on the jet axis at a distance x from the propeller plane. Velocities and the axial distance are referenced to the efflux velocity v_o and the design propeller diameter D_p	36

List of Tables

Table 2-1. Present CCSC dimensions near the ferry.....	19
Table 3-1. Typical values of C_b at fully loaded drafts (Cult of Sea, 2018).	28
Table 3-2 Model navigation vessel and channel parameter values.....	32
Table 3-3. Maximum mean water depth reduction Δh due to drawdown and associated coefficients evaluated at a longitudinal distance l_x from section E-E'.	33
Table 3-4. Maximum average return current and associated coefficients evaluated at a longitudinal distance l_x from the section E-E'.	34
Table 3-5. Maximum wave height H_m and associated coefficients evaluated for a cross-sectional area A_c located a longitudinal distance l_x from the section E-E' and lateral distance y from the channel centerline...	34
Table 3-6. Design parameters used to calculate propeller-wash flow velocities.	35
Table 3-7. Efflux velocity v_0 and associated coefficients.....	35
Table 3-8 The maximum main velocity at various shallow water depths.	36
Table 3-9. Maximum near-bed velocities at various water depths below the propeller main axis.	37

1. INTRODUCTION

1.1. Background

TXDOT is interested in identifying potential impacts to the Port Aransas Ferry (ferry) system (operations and infrastructure) stemming from the proposed Corpus Christi Channel Improvement Project (CCCIP). This proposed project is funded jointly by the Port of Corpus Christi Authority (PCCA) and the federal government (USACE, 2003). Additional plans include deepening the Corpus Christi Ship Channel (CCSC) to depths of between 78 and 80 feet, from offshore to the location of the ferry landing. This is requested to accommodate Very Large Crude Carriers (VLCC) at a planned facility on Harbor Island, immediately east of the ferry Harbor Island landing site. CCCIP consists of navigation improvements and environmental restoration components to be completed by the end of 2021. The timeline for the remainder of the modifications is not completely finalized yet. This study focuses on assessing potential impacts that the CCCIP, additional deepening, and the presence and movement of the VLCCs have on ferry operations and associated infrastructure (Figure 1-1).

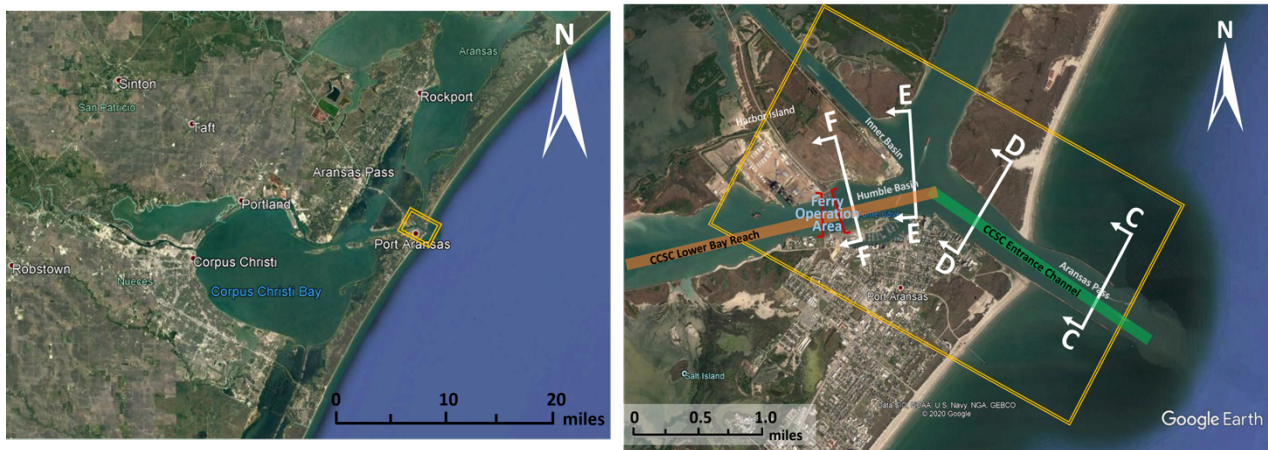


Figure 1-1. Port Aransas ferry study area.

1.2. Proposed Modifications in the Vicinity of the Ferry Terminals

1.2.1. Channel Deepening to 54 feet below MLLW

The navigation improvement plan of the CCCIP includes deepening to 52 feet below MLLW the CCSC in the Inner Harbor to the end of the jetties in the Gulf of Mexico. The plan also includes deepening the remainder of the channel into the Gulf of Mexico to 54 feet below MLLW; widening the Upper Bay and Lower Bay reaches to 530 feet; construction of parallel, 12-foot deep barge shelves across the Upper Bay portion of the CCSC; and extending the La Quinta Channel approximately 7,400 feet to a depth of 39 feet (USACE, 2003). A schematic of the current CCCIP layout and schedule is provided in Figure 1-2. Accordingly, the impact on the ferry operation area is investigated based on the plan to deepen the main ship channel in the Lower Reach from its current depth of 47 feet to 54 feet below MLLW and widening it from 400 feet to 530 feet, respectively.

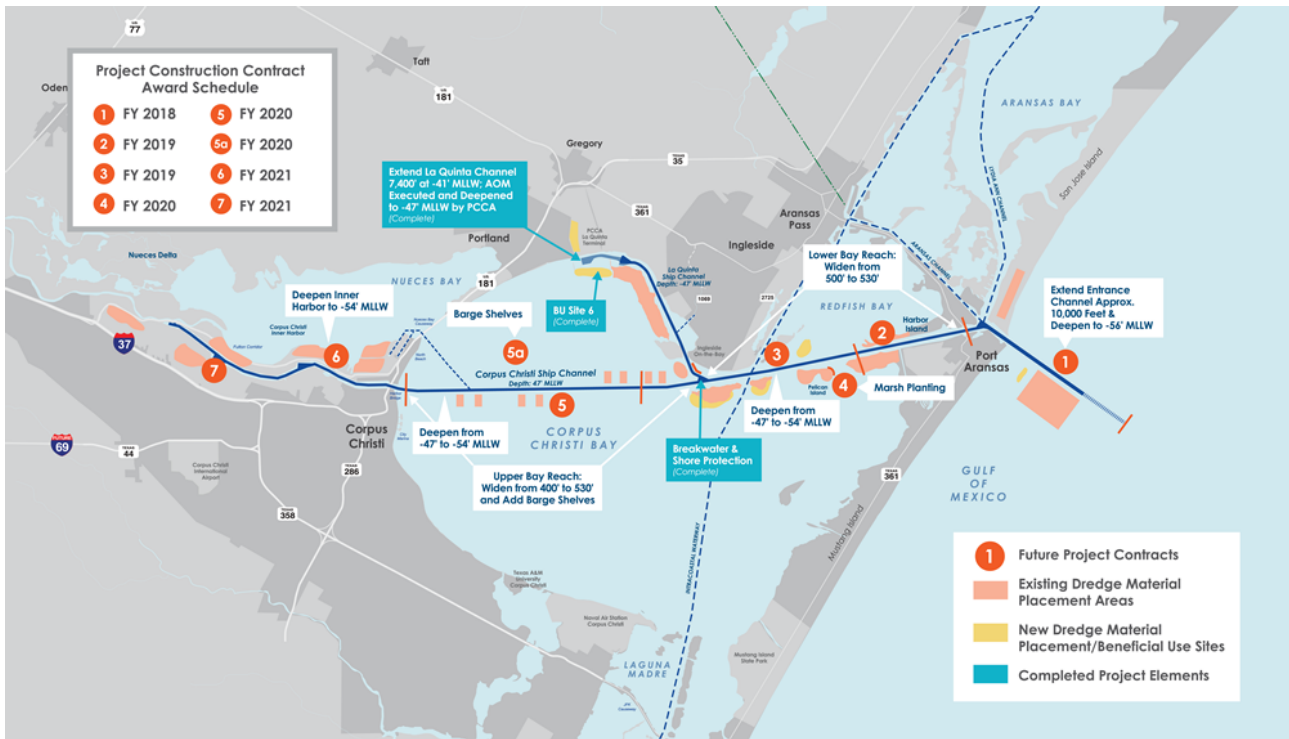


Figure 1-2. Current CCCIP construction layout and project schedule (Port of Corpus Christi Authority, 2018).

1.2.2. VLCC Terminal Installation on Harbor Island

PCCA is proposing the construction of two berths that require dredging and excavation along the southern portion of Harbor Island ("VLCC Facility Project") as depicted in Figure 1-3. The proposed berths are referred to as Berth 1 and 2, respectively. Berth 1 and Berth 2 are intended to cut into the Island at an approximate 45-degree angle to the CCSC. The berth structures will consist of shoreline protection, including articulated block mats, bulkheads, a cellular wall, breasting structures, jetty platforms, and access structures, etc. The project area covers approximately 64.8 acres of the terminal basin. The two berths will be in an area currently occupied by three existing berths which are damaged and unusable, and which are in the process of being demolished (Wood Environment & Infrastructure Solutions, Inc., 2019).

The new berths will be dredged to a depth of 60 feet below MLLW (54 feet below MLLW plus four feet of advanced maintenance and two feet of allowable over-dredge) to match the currently authorized channel. The CCSC currently ranges from a 47-ft depth in the Lower Bay segment to a 49-ft depth in the entrance channel and is authorized to a depth of 54 feet below MLLW. The VLCC Facility Project will generate approximately 6,500,000 CY (cubic yards) of dredge material and excavation.

A cellular bulkhead wall is planned between the northern TXDOT ferry landing and the new terminal basin. This wall will be installed on the eastern side of the existing bulkhead wall and will be immediately adjacent to it. Publicly available plans show that the new wall will extend the same distance toward the CCSC as the existing wall, although the possibility to extend it further (i.e. an

extra 50 feet) exists. Further possible modifications to the extended wall design include perforation via inclusion of gaps.

Once completed, the project will provide the first Texas port with the ability to operate two-way marine traffic in the CCSC at a depth below 50 ft MLLW from the Gulf of Mexico to the ferry landing. The ships will enter through the Aransas Channel west of Port Aransas with the help of tugboats, then make a left turn into the CCSC, while in front of the terminal they will be turned 180 degrees and backed into the berths. Once loaded, the ships will be able to immediately enter the CCSC, line up with the Aransas Channel and exit to the Gulf of Mexico. The Harbor Island terminal will be a full-service crude oil export facility with the ability to load VLCC ships.

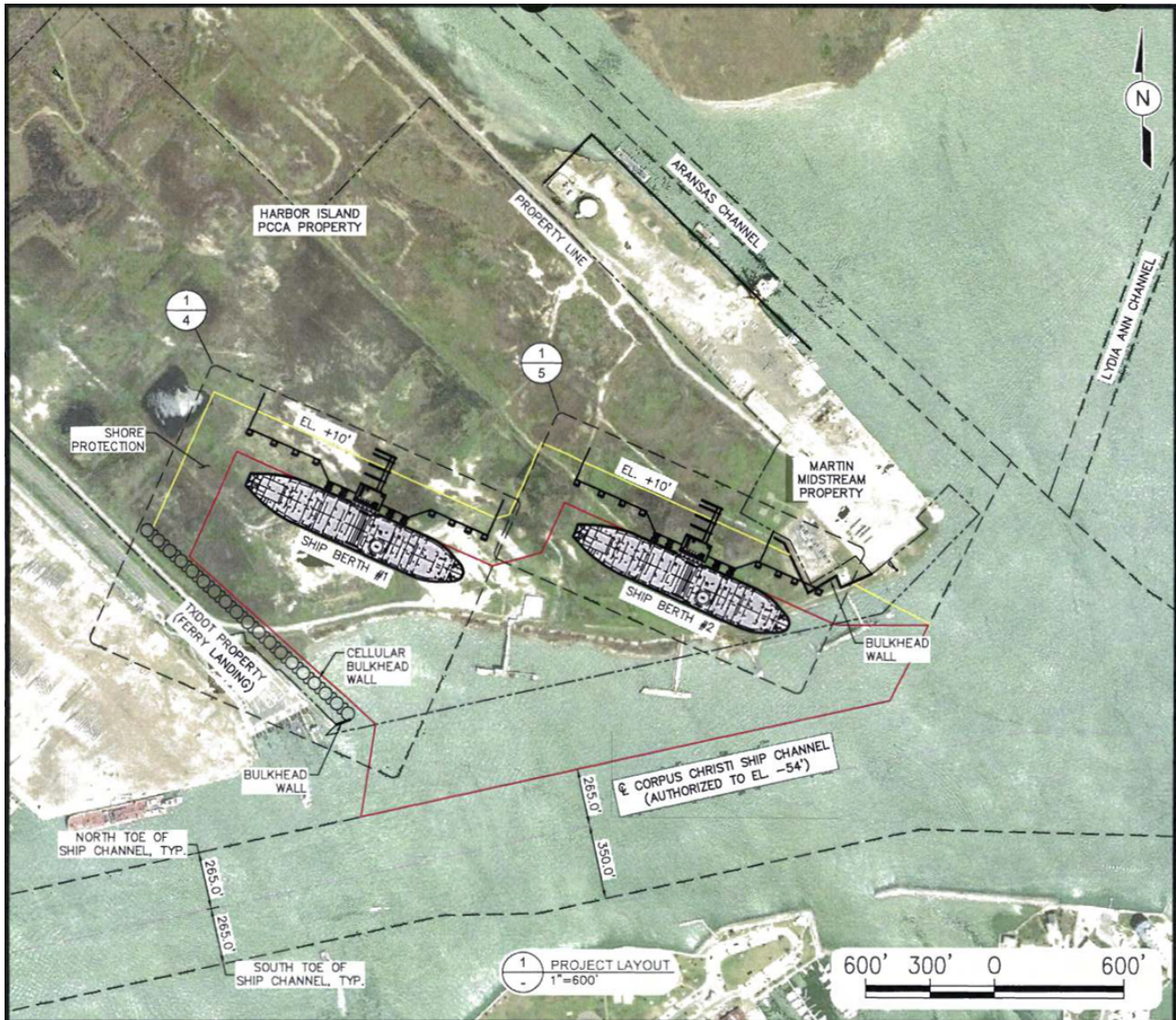


Figure 1-3. Project site plan for two berth structures of the new VLCC terminal proposed to be constructed in the southern portion of Harbor Island in Nueces County, Texas (Source: Wood Environment & Infrastructure Solutions, Inc., 2019).

1.2.3. Channel Deepening to 79 feet below MLLW near the Ferry

The Entrance Channel is defined as that portion of the CCSC extending from Station -310+00 in the Gulf of Mexico to Station -37+82 (north to transect C-C in Figure 1-4) in the Inner Basin. PCCA requested permit authorization from the U.S. Army Corps of Engineers (USACE) – Galveston District (SWG) to conduct deepening of the portion of the Entrance Channel (from Station 54+00) and extension into the Gulf of Mexico (Station -620+00) as show in Figure 1-4. The CCSC is currently authorized by the USACE to depths of 54 feet below and 56 feet below MLLW from Station 54+00 to Station -330+00 as part of the CCCIP. The current authorized width of the CCSC is 600 feet inside the jetties and 700 feet in the entrance channel. The additional proposed project would further deepen the channel from Station 54+00 to Station -72+50 to a maximum depth of 79 ft below MLLW (75 ft plus two feet of advanced maintenance and two feet of allowable over-dredge). Likewise deepening from Station -72+50 to Station -330+00 to a maximum depth of 80 ft below MLLW (77 ft plus two feet of advanced maintenance and one foot of allowable over-dredge) is proposed. The planned project includes a 29,000-ft extension of the CCSC from Station -330+00 to Station -620+00 to a maximum depth of 80 ft below MLLW (77 ft plus two feet of advanced maintenance and one foot of allowable over-dredge) to reach the 80-ft below MLLW bathymetric contour in the Gulf of Mexico. The overall project length is approximately 12.8 miles.



DREDGING PLAN
SCALE: 1" = 8000'

SEGMENT	STATIONING (@ CHANNEL CL)		*DEPTH (FT BELOW MLLW)	DESCRIPTION	PLAN VIEW LEGEND
	FROM	TO			
1	STA -620+00	STA -330+00	-77.0	Outer Channel	[Blue Box]
2	STA -330+00	STA -72+50	-77.0	Approach Channel	[Light Blue Box]
3	STA -72+50	STA -15+08.24	-75.0	Jetties to Harbor Island Transition Flare	[Green Box]
4	STA -15+08.24	STA 19+48.10	-75.0	Harbor Island Transition Flare	[Light Green Box]
5	STA 19+48.10	STA 38+16.42	-75.0	Harbor Island Junction	[Yellow Box]
6	STA 38+16.42	STA 110+00	-75.0	Corpus Christi Channel	[Orange Box]

* DESIGN DEPTH SHOWN. DOES NOT INCLUDE 2.0 FT ADVANCED MAINTENANCE DREDGING OR 2.0 FT ALLOWABLE OVER DREDGE.

Sheet 2 of 23

Corpus Christi Ship Channel Deepening Project
Individual Permit Application SWG-2019-00067

Preferred Channel Alternative

County: Aransas and Nueces
Application By: Port of Corpus Christi Authority

State: Texas
Date: May 2019

Figure 1-4. Proposed dredging plan for deepening and extending the portion of the CCSC from Harbor Island into Gulf of Mexico to the maximum 80 feet below MLLW (AECOM, 2019).

The proposed project also involves the placement of fill (dredged material) in waters of the United States. Both of the proposed activities are regulated by the USACE. The proposed maximum 80-ft deepening project is needed to accommodate transit of fully laden VLCC vessels that draft approximately 70 feet. The proposed project does not include widening the channel, however, some minor incidental widening of the channel slopes is expected in order to meet side slope requirements and to maintain the stability of the channel.

1.3. Vessels, Facilities, and Operations

1.3.1. VLCC Specifications

Currently, crude oil is exported using Aframax and Suezmax size vessels. The Suezmax vessels are sometimes light loaded (lightered) due to depth restrictions in the existing CCSC, and would continue to be light loaded when the current federal authorized CCSC deepening project (to 54 ft below MLLW) is completed. However, the current channel depth requires that large crude carriers remain offshore and transfer their cargo into smaller crude tankers (e.g., ship-to-ship transfer) in the Gulf of Mexico for the remainder of the voyage. To efficiently and cost effectively move crude oil cargo, oil exporters are increasingly using fully loaded vessels, including VLCCs (see Figure 1-5). Non-liquid commodity movements are also trending toward larger, more efficient vessels. The proposed additional deepening to 79 feet below MLLW and VLCC terminal construction projects were intended to accommodate and improve the efficiency of the deep-draft navigation system. The dimensions for a typical VLCC are assumed as 1,188 ft (362 m) in length, 228 ft (70 m) in width (i.e. beam width), and 95 ft (29 m) in depth with a possible draft of 74 ft (23 m). Further assumptions include the maximum speed through a confined shipping channel of 11 knots (5.7 m/s), a block coefficient C_b of 0.84, and a propeller diameter of 31.5 ft (9.6 m) (USACE, 2006). Since no Automated Information System (AIS) data for VLCC vessels traversing the CCSC exist, the focus of the impact analysis is on identifying potential impacts to ferry operations resulting from VLCC vessels with the aforementioned dimensions and parameters traversing the CCSC dredged to 78 feet below MLLW.



Figure 1-5. Photo of a VLCC for illustration purposes.

1.3.2. Ferry Landing Structures

Both ferry terminals (Harbor Island and Mustang Island) currently feature five adjacent ferry landings each with ramps, fenders, and pile clusters to facilitate ferry berthing, loading, and unloading. The Mustang Island facility also features an additional maintenance berth (westward one) that is not used for vehicle transfers. The typical minimum width of a landing between the most shoreward tower piles is 18 feet 9.5 inches. The ferry landings widen toward the CCSC to facilitate ferry docking and are protected against ferry impacts with fenders affixed to wood pile clusters. As an example, Figure 1-6 displays a portion of a planview blueprint of a typical landing on the Mustang Island side.

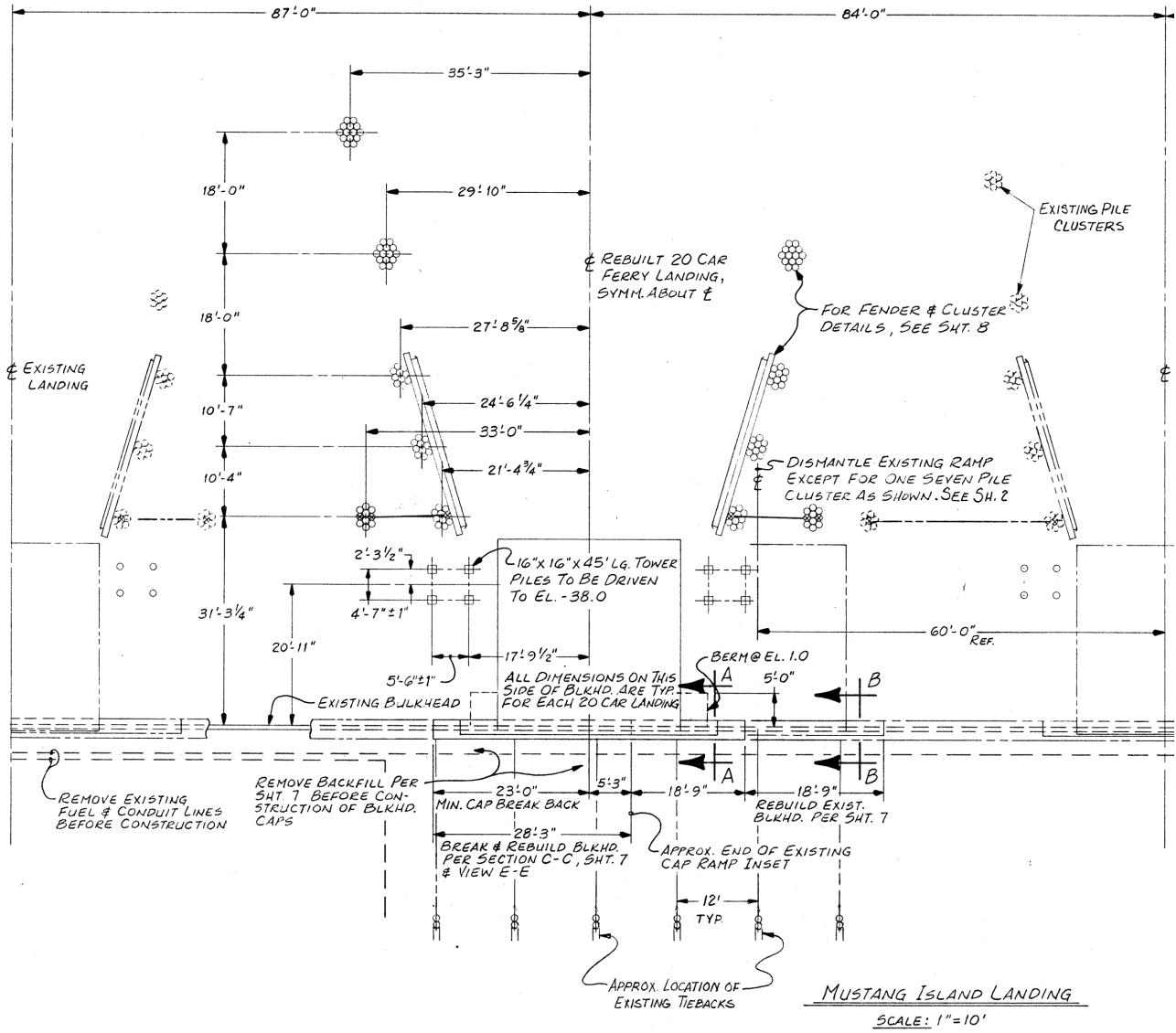


Figure 1-6. Planview of Mustang Island landing blueprint excerpt (source: TXDOT).

Rubble mound slopes (1:1) of 3-foot thickness protect the earthen slopes at each landing from erosion down to a depth of approximately 10 feet below MLLW (Figure 1-7). The rubble-mound berm-crest elevation is set at around 1 foot above MLLW. Bulkhead sheet pile with concrete caps and tieback rods make up the vertical sections of the landing structures and extend, at a minimum, down to 20 feet below MLLW. The bottom elevation at the bulkheads is approximately 8 feet below MLLW based on construction blueprints. Of course this value can vary based on local hydrodynamics, scour and sedimentation processes.

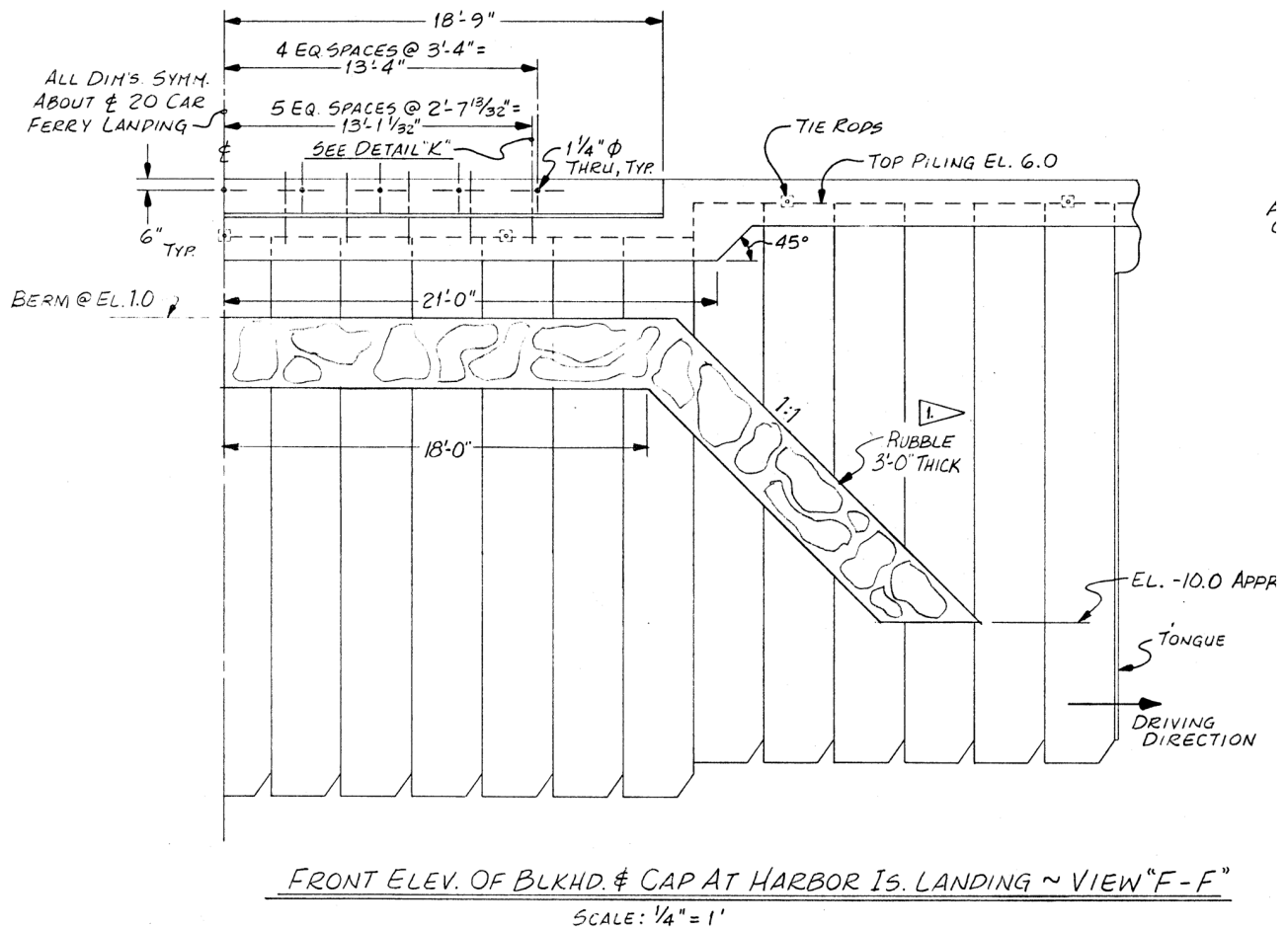


Figure 1-7. Elevation side view of Harbor Island landing blueprint excerpt showing the front elevation of the bulkhead and cap (source: TXDOT).

1.3.3. Ferry Vessels

Three different ferry vessel sizes make up the existing Port Aransas TXDOT fleet. These include 9-car, 20-car, and 28-car models. The latest addition to the fleet are two new 28-car ferry vessels (Figure 1-8) for which TXDOT provided detailed specifications (Figure 1-9). The principle dimensions include an overall length of 159'7", a length at the water line under design load of 153'6", a length between perpendiculars of 145'0", a beam width of 52'0", a depth at the side of 13'5", and a draft of 5'0". These vessels feature single propeller engines on both ends of the vessel to avoid the necessity of any turning maneuvers.



Figure 1-8: Photo of new 28-car passenger ferry Amadeo Saenz Jr (photo: TXDOT).

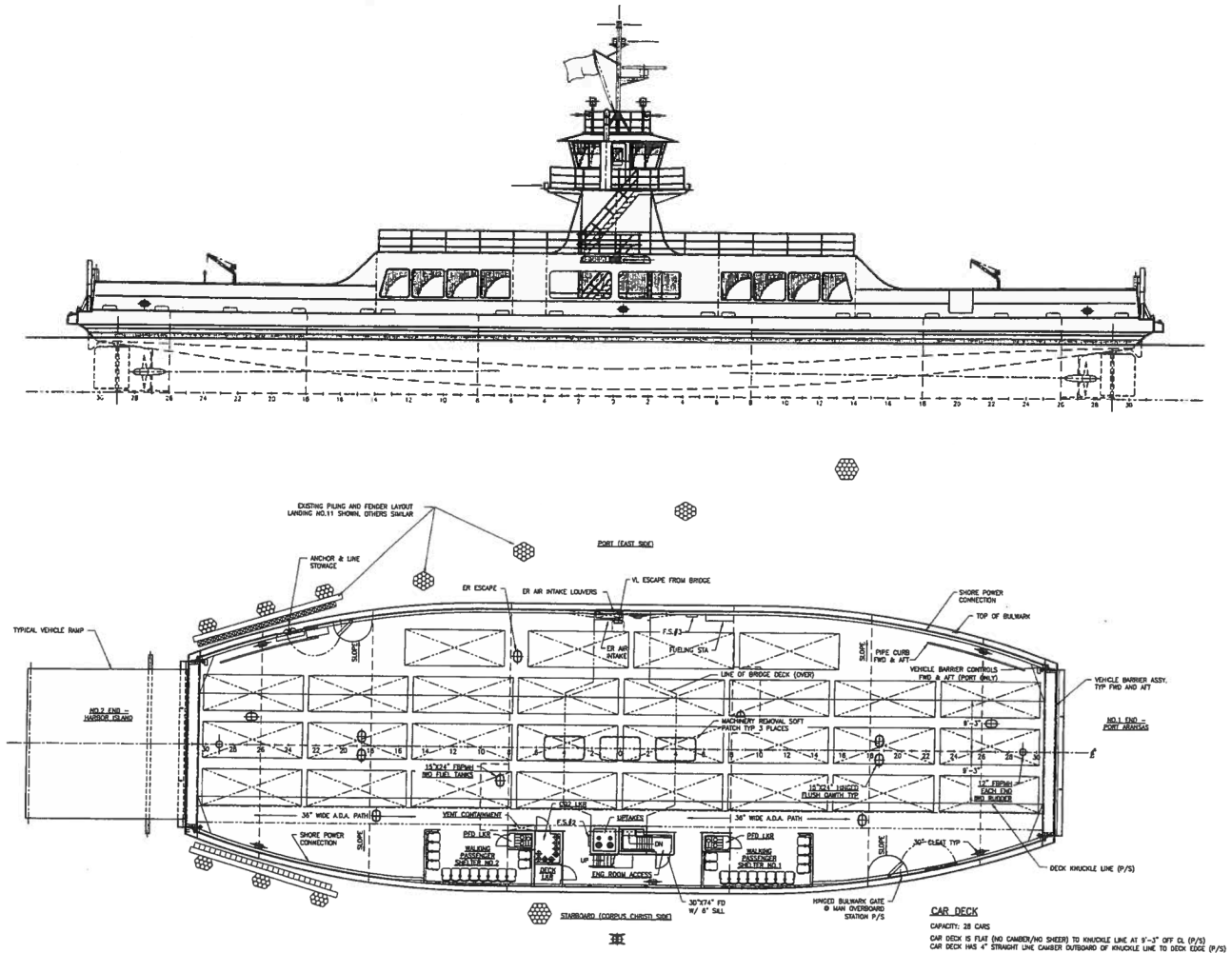


Figure 1-9. Schematic of outboard profile (top) and deck planview (bottom) of 28-car ferry type (source: TXDOT).

The 20-car ferries are only slightly smaller than the 28-car ones described here. The 9-car ferries are about 100 feet in length and 44 feet in beam width.

1.3.4. Ferry Operations and Regulations

The Port Aransas route operated by TXDOT runs two vessels placed in service at 6:30 a.m. After this departure, the two vessels operate based on traffic volumes, and trips are spaced to carry traffic as efficiently and safely as possible. A third vessel is placed in service during the afternoon period as necessary. Up to six vessels may be operated for summer and holiday traffic. Hazardous conditions caused by strong winds, associated currents and large waves can capsize or damage vessels. When adverse weather condition exists, vessel operations may be suspended until conditions improve. Safe

operating conditions for a vessel are determined by the Captain based on information obtained from the Port Aransas Ferry Operations Manager. Adverse local weather conditions resulting in temporary suspension of ferry operations include sustained winds over 39 mph, and/or forecast swells of 6 feet or greater, as well as the approach of a strong northern, or extreme thunderstorm with frequent lightning strikes close to the ferry location. In such conditions, the Small Craft Advisory is issued by the Coastal and Great Lakes Weather Forecast Offices (WFO) for areas included in the Coastal Waters Forecast or Nearshore Marine Forecast (NSH) products (NOAA, 2020; US EPA, 2012). In addition, orders for suspension of operations come from the Captain of the Port (U.S. Coast Guard) via email through the Marine Safety Information Bulletin (MSIB).

Certain size and weight restrictions exist for vehicles wanting to board the ferries. Combined vehicles, such as trucks towing a boat, may not be longer than 80 feet, wider than 13 feet or taller than 13 feet 6 inches. Single-axle vehicles may weigh no more than 20,000 pounds, tandem axles no more than 34,000 pounds and combination vehicles may not exceed a total of 80,000 pounds. Vehicles should not exceed 80,000 pounds, may have a maximum length of 65 feet, a maximum height of 13.5 feet and a maximum width of 8.5 feet (TXDOT, 2020).

2. EXISTING ENVIRONMENTAL CONDITIONS

2.1. Datums

The horizontal datum for this study is based on the Texas State Plane Coordinate System, South Central Zone 4204, North American Datum of 1983 (NAD83). The vertical datum is MLLW in feet. All prior projects in the Galveston District have used the USACE vertical datum MLT (Mean Low Tide). The USACE has completed the process of converting the vertical datum for all navigation projects from MLT to MLLW (USACE, 2016, 2015). MLLW is 0.15 feet below MLT and 0.12 feet below the North American Vertical Datum of 1988 (NAVD88).

2.2. Coastal Climate

Water circulation in the relatively shallow water basin of Corpus Christi Bay is forced by both marine and atmospheric processes. The atmospheric processes are driven by fluctuations in temperature, precipitation, and winds, while the major marine processes involve variations in waves, tides, water temperature, salinity, and flow contributions from tributaries and overland runoff. Tropical storms and hurricanes as well as cold fronts can affect all of these processes. Increased wave activity and deviations from normal water levels are a common result.

The tides and the currents produced by the gravitational pull of the moon and sun acting on a rotating earth are responsible for about 50% of the marine energy delivered to the coast. The major impact of tides is to shift the shoreline between high and low tide, and to generate tidal currents parallel either to the coast, or at tidal inlets and estuaries. Waves provide about half the energy to do work at the coast. Winds blowing over the oceans are responsible for energy that generates waves which transport and release kinetic energy as they shoal and break on the coast. The stronger the wind, the longer it blows and the longer the fetch (i.e., a stretch of ocean over which wind blows), the larger the waves. Occasional hurricanes can produce large waves and storm surge. Seabed erosion frequently occurs during the high (flood) tide, whereas seabed deposition occurs during ebb tide in the long, tidally influenced channels. The narrow entrance channel connecting the large bay with the ocean will experience significant velocity gradients between daily high and low tides that impose shear stress on the bottom and banks of the channel. Waves generated by wind can produce a bottom shear stress approximately equivalent to that induced by tidal currents (Cox et al., 2017; Dean and Dalrymple, 2001; Short, 2012).

Both tidal currents and prevailing winds can have a significant effect on surface temperatures and water salinity. Temperature and salinity can create vertical, density-driven water circulation and stratification beneath the sea surface where it tends to keep the denser, colder water on the bottom and warmer, less dense water on top. The main processes that increase seawater density are cooling, evaporation, and ice formation and those that decrease seawater density are heating and dilution by fresh water through precipitation, ice melting, or fresh water runoff. Water movements caused by a change in the density-driven circulation in the coastal shallow water system can transport organisms, circulate nutrients and oxygen, transport sediment and pollutants, and influence the mean sea surface position. The average seasonal cycle of mean sea level elevation can also be caused by regular fluctuations in coastal temperatures, salinities, winds, atmospheric pressures, and ocean currents (Webb, 2019; Wolanski, 2007; Huthnance, 1995, 1981).

Information on offshore tidal water level, local wind, precipitation, and seawater and air temperatures were obtained from a nearby NOAA CO-OPS station located at Port Aransas, TX (Station ID# 8775237; Figure 1-1).

2.2.1. Tidal Water-Level Fluctuations

Figure 2-1 shows the offshore tidal water level observed throughout the year 2019. The project area experiences diurnal tides where one high and low tide occur during each daily tidal cycle. Mean and diurnal tidal ranges are 0.89 and 1.04 feet, respectively, and mean tide level is at the elevation of 0.57 feet above MLLW. Elevated tidal surge is experienced during storm conditions and high spring tide events, and the spring storm tidal water level can reach 3 feet (nearly 1 meter) above MLLW, for example, in 2019 (Figure 2-1).

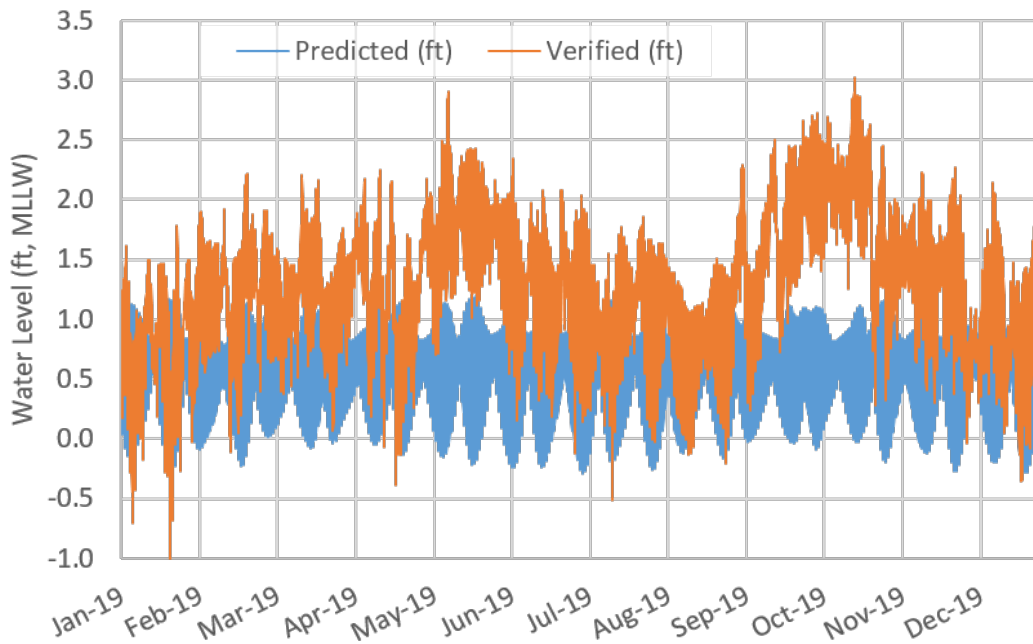


Figure 2-1. Tidal water levels observed near the ferry system in 2019. The hourly water level time series was obtained from nearby NOAA CO-OPS Station at Port Aransas, TX (8775237).

2.2.2. Winds

Figure 2-2 provides the annual time series and statistical distribution of speed and direction of winds in the Port Aransas area. Wind speed (in knots) is the scalar average of wind speeds measured approximately at 30 ft (9 m) above MLLW over a two-minute period prior to each tenth of an hour (i.e., 6 minute interval). Wind direction is the vector average of the wind used for wind speed calculations and refers to the direction the wind is coming from in degrees clockwise from true north. The wind record from the year 2019 shows that more than 90% of annual wind speed fell within the 5.0 – 15.0 knots (2.6 – 7.7 m/s) range, and that wind blew most prevalently from a direction of 105 – 195° (ESE – SSW).

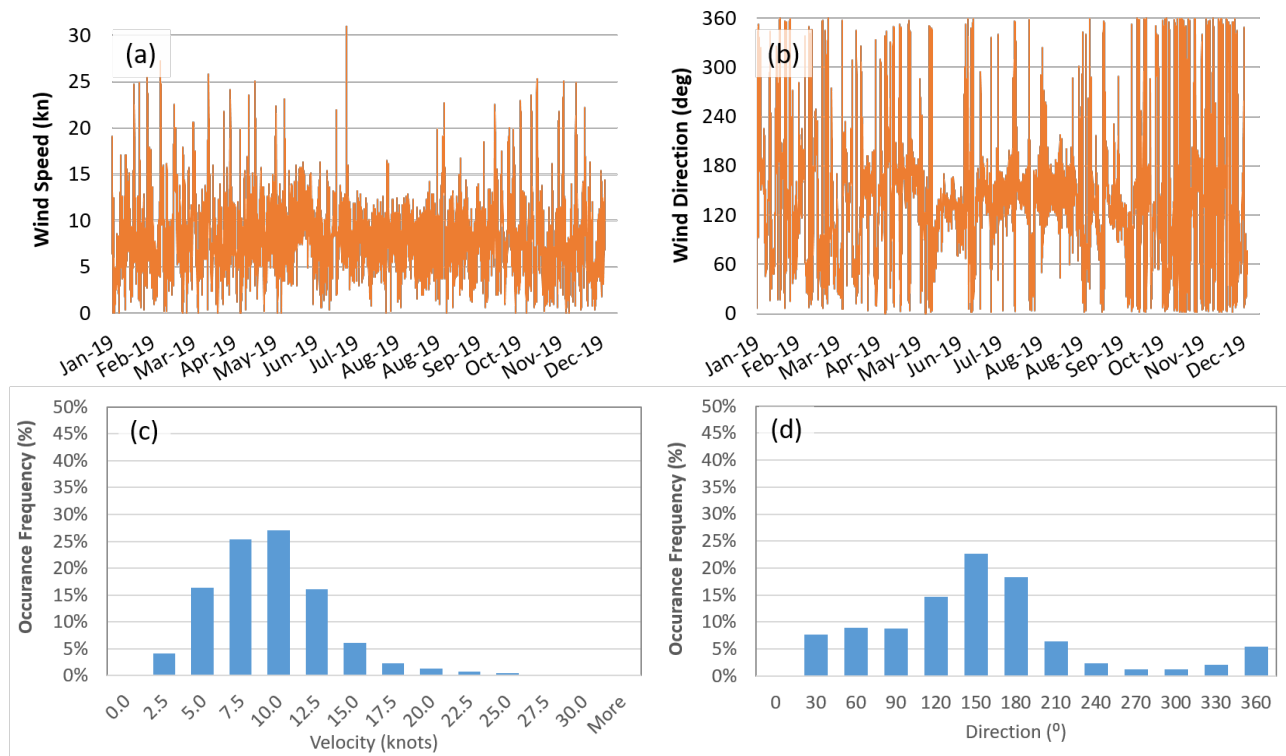


Figure 2-2. Hourly wind observed in the Port Aransas area during 2019. The upper and lower panels show annual time series and statistical distributions, respectively, of speed (a, c) and direction (b, d) of the local wind. Direction indicates where wind is coming from in degrees clockwise from true north.

2.2.3. Waves

Wave information at the ferry site is extracted from a recent USACE modeling report (USACE, 2018) since wave field measurements at the ferry site itself are not available. Three typical wind conditions representing southeasterly (April 2017), southerly (20 July to 20 August 2017), and northerly (December 2017) winds, respectively, were used as input forcing to the spectral wave module of the numerical Coastal Modeling System – CMS (Demirbilek and Rosati, 2011; Lin et al. 2008, 2011, Buttolph et al., 2006). In addition, a 10-day simulation of wave, current, and water level changes including the impact of Hurricane Harvey in 2017 was conducted (21-31 August 2017). All simulations were carried out for present conditions and for a 50-year sea level rise (SLR) value of +0.573 m, respectively, to investigate the impact of increased water levels on hydrodynamics. The southerly wind and Harvey conditions were also simulated for the bathymetry resulting from the authorized CCCIP (i.e. deepening of the CCSC to 54 ft below MLLW) to check its impact on hydrodynamics (both with SLR and without).

The following is a summary of the wave information computed for the numerical model output station in the center of the CCSC directly at the ferry site. In general, waves entering the CCSC from the GOM are drastically reduced due to channel geometry, jetties, and wave attenuation by energy dissipation. The location of the ferry terminal exhibits some of the lowest wave heights along the entire CCSC, mainly due to its distance from both the jetty entrance and the more open waters of the bay. The maximum significant wave height for the representative southeasterly, northerly, and Hurricane Harvey wind forcing was 0.13 m, 0.12 m, and 0.21 m, respectively. These values did not change due to the CCCIP deepening efforts indicating that the ferry location is not susceptible to wind

wave height changes caused by channel deepening.

2.2.4. Currents

Field measurements of currents in the vicinity of the ferry terminal are scarce. However, in 2019 a Texas A&M field campaign did survey the area with a vessel-mounted acoustic Doppler current profiler (ADCP). In the following, data from that campaign are summarized. These represent normal conditions. Figure 2-3 and Figure 2-4 show velocity vectors of the mean current U_{95} along a 5000 m (~ 3 mile) stretch of CCSC between southern Harbor Island and northern Port Aransas during slack to ebb and flood to slack tidal stages, respectively. The raw velocity data were processed to calculate average speed and direction of U_{95} . U_{95} was computed by first averaging the raw velocity ensembles within 95% of the total water depth from the surface at each time and location, and then by taking the moving average of the depth-averaged velocities with a 1-second window (i.e., average of two depth-averaged velocity ensembles with 2 Hz sampling rate applied for the current measurement). Every 25th mean current velocity vector (~12 seconds) is displayed in the figures.



Figure 2-3. Depth-averaged current (U_{95}) during slack to ebb tidal stage in the CCSC between Harbor Island and Port Aransas. (a) Spatial and (b-c) statistical distributions of speed and direction of U_{95} . The direction of U_{95} refers to the current heading measured clockwise from true north. Field current measurements were conducted on September 22, 2019, from 11 AM to 12 PM.

The average mean current U_{95} during ebb tides in the ship channel adjoining the Port Aransas and Harbor Island area varied mostly between 0.5 and 1.0 m/s and average speed of U_{95} was 0.7 m/s. The prevalent current heading was toward 75° (ENE) - 165° (SSE), in line with the orientation of the ship channel in the area. The average mean current U_{95} during flood tides varied mostly between 0.1 and 0.3 m/s and the average speed of U_{95} was 0.2 m/s. The prevalent current heading was toward 255° (WSW) - 345° (NNW), in line with the orientation of the ship channel in the area.

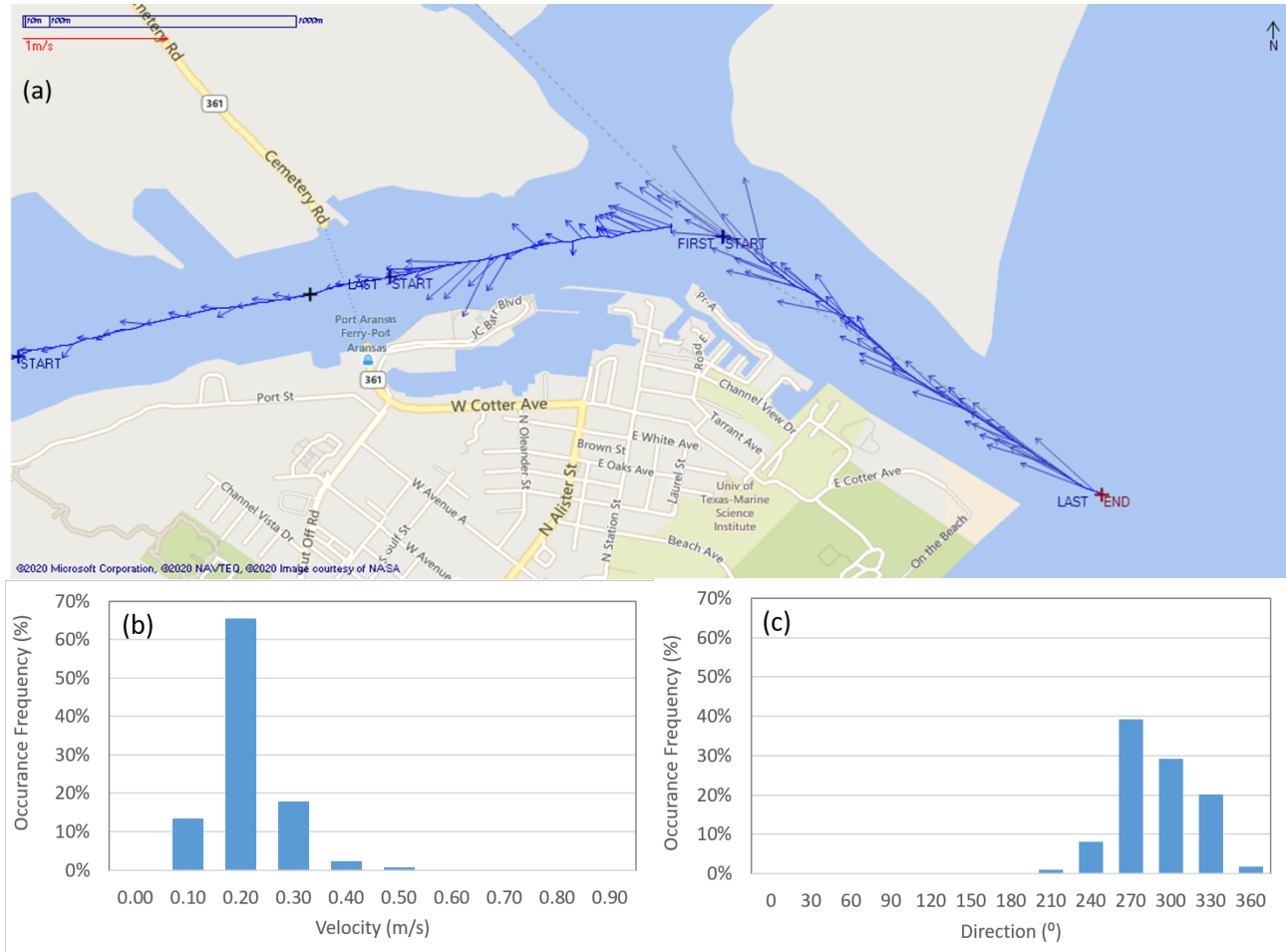


Figure 2-4. Depth-averaged current (U_{95}) during flood to slack tidal stage in the CCSC between Harbor Island and Port Aransas. (a) Spatial and (b-c) statistical distributions of speed and direction of U_{95} . The direction of U_{95} refers to the current heading measured clockwise from true north. Field current measurements were conducted on September 26, 2019, from 3 PM to 5 PM.

The modeling study introduced in the previous section also provided data on currents (USACE, 2018). At the ferry location the maximum current for the representative southeasterly, northerly, and Hurricane Harvey wind forcing conditions was 0.678 m/s, 1.696 m/s, and 0.785 m/s, respectively, using the channel geometry prior to any deepening efforts. Once the CCCIP deepening was included in the simulations, these values reduced slightly to 0.621 m/s, 1.540 m/s, 0.727 m/s. This indicates that deepening the channel near the ferry location generally reduces currents, which can mostly be attributed to flow volume conservation since the same flow rate now encounters an increased cross-sectional area.

2.2.5. Precipitation and Temperature

Seasonal changes in temperature can be most easily detected in the coastal regions of the mid-latitudes, where surface temperatures are at a minimum in winter and reach maximum values in late summer. Generally, the Corpus Christi Bay area experiences peaks in rainfall amounts between May and July as well as September and October based on averages recorded between the years 1981 and 2010. Based on those data, average monthly cumulative precipitation exceeds 3 inches in those months as shown by the orange bars in Figure 2-5a. The year 2019 was somewhat different from that trend. The May precipitation rate was double, whereas July showed barely any precipitation at all (blue bars in Figure 2-5a). December rainfall amounts were more than double the historic average value. The annual distribution of air and water temperatures recorded during 2019 indicates that the surface water temperature of the adjacent CCSC reached nearly 90 °F during summer and varied between 50 and 70 °F during the winter. The air and sea surface temperatures were measured at sensors positioned at elevations of 23 feet above MLLW and 5 feet below MLLW, respectively.

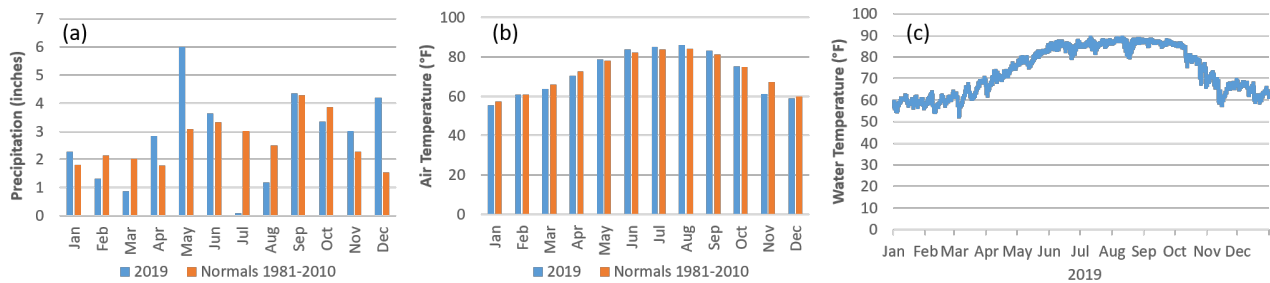


Figure 2-5. Rainfall amount, air, and water temperature observed near the ferry system. The annual precipitation (a) and air and water temperature (b and c) were obtained from the NOAA CO-OPS Station Port Aransas, TX (8775237).

2.2.6. Sea Level Trends

The average seasonal cycle of mean sea level and local relative sea level (RSL) trend in the Corpus Christi Bay area are given in Figure 2-6. The average mean sea levels were calculated from the monthly mean sea level data obtained from 1983 to 2019 at the long-term water level station located offshore Corpus Christi Bay (Station #: 8775870). The seasonal cycle of mean sea level shown along with each month's 95% confidence interval in Figure 2-6a is caused by regular fluctuations in coastal ocean temperatures, salinities, winds, atmospheric pressures, and currents. The RSL trend is obtained from tide gauge records with respect to a local fixed reference on land and a combination of the local sea level rise or fall and the local vertical land motion. The long-term linear trend in RSL, including its 95% confidence interval, shown in Figure 2-6b is calculated using a minimum span of 30 years of station data averaged by month in order to eliminate the effect of higher frequency fluctuations and hence to compute the linear sea level trend.

Mean sea level tends to fluctuate not only in the long-term, but also on a monthly basis. For Corpus Christi, peaks of mean sea level are usually observed in May (0.04 m / 0.13 ft above annual mean) and in October (0.16 m / 0.53 ft above annual mean) as shown in Figure 2-6 where the monthly mean values between the years of 1983 and 2019 have been used. The long-term RSL trend in the Corpus Christi Bay area is 5.11 mm/year with a 95% confidence interval of +/- 1.06 mm/year, which is equivalent to a change of 1.68 feet in 100 years (Figure 2-6).

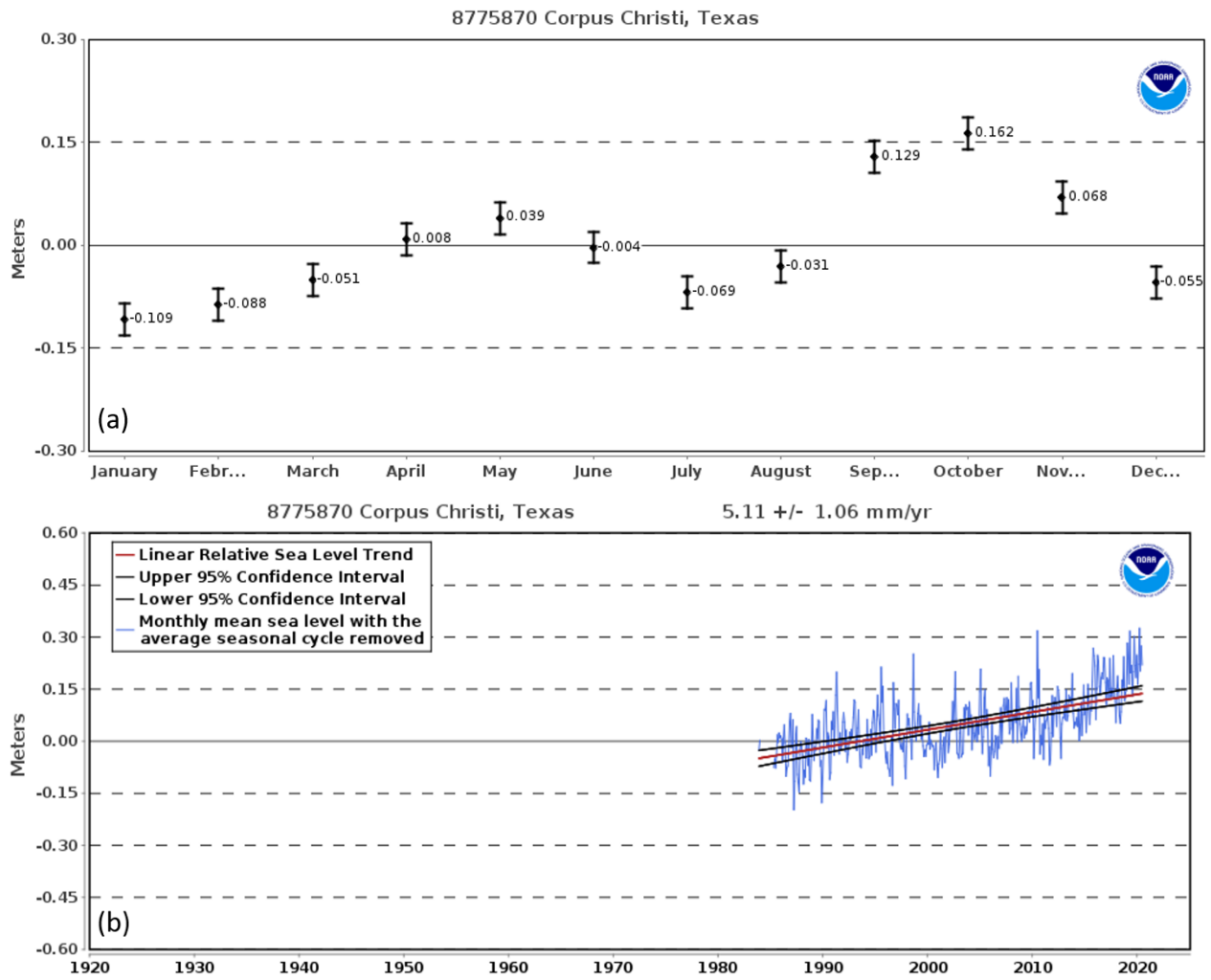


Figure 2-6. Average seasonal cycle of average mean sea levels (a) and RSL (Relative Sea Level) trend (b) estimated for the Corpus Christi Bay area. Monthly mean sea level data between 1983 and 2019 were obtained from the long-term water level station located offshore Corpus Christi Bay (Station #: 8775870). The 95% confidence intervals in the seasonal mean seal level and linear trend in RSL are calculated using a minimum span of 30 years of station tide data averaged over each month.

2.3. Channel Geomorphology and Sediments

The CCSC begins in deep water in the Gulf of Mexico about three miles offshore, passes through the jettied inlet at Port Aransas, and extends about 21 miles westward into Corpus Christi Harbor (Figure 1-1). The current study area includes two segments: the Entrance Channel and the Lower Bay reach. The Gulf of Mexico and the Inner Basin are the boundaries of the Entrance Channel. The jetties that protect the Entrance Channel are 11,190 and 8,610 feet long and extend into the Gulf to stabilize the inlet at Aransas Pass. The Lower Bay reach extends westward of the Inner Basin, is mostly landlocked between Harbor Island and Port Aransas, and is separated from the Upper Bay by the La Quinta Channel Junction (Figure 1-1).

The landlocked portion of the Entrance Channel is 700 feet wide and will be deepened to 52 feet plus 2 feet of advanced maintenance. The entrance toward the open waters of the Gulf will be dredged to a 54-foot authorized depth with two feet of advanced maintenance. The existing channel dredge template for the 54-ft depth of the CCCIP will require widening by 100 feet on the northern side of the channel. This will improve the turning radius for vessels passing through the Entrance Channel and making the turn either out to the Gulf or into the Lower Bay portion of the channel. The Lower Bay portion of the CCSC in the study area will be deepened from 45 feet to 52 feet plus 2 feet of advanced maintenance. The current design width for this portion of the channel is 530 feet. Currently, the western portion of this channel segment is wider than the selected 530 feet, and will remain as is. The additional proposed deepening to a maximum depth of 78 ft below MLLW will affect both study segments near the ferry system by dredging the channel extent from Station 54+00 (i.e. Bayside of section FF in Figure 1-1) to Station -72+50 (i.e., seaside of section CC). Berths of the proposed VLCC terminal will be constructed adjacent to the landside of section FF. The surveyed CCSC bottom positions are illustrated together with existing (54-ft MLLW) and proposed (78-ft MLLW) channel dredge templates at selected cross-sectional positions (CC – FF) in Figure 2-7. The current CCSC dimensions are summarized in Table 2-1.

Table 2-1. Present CCSC dimensions near the ferry

CHANNEL SEGMENT	Depth (ft)	Width (ft)	Length (mi)
Entrance Channel			
Aransas Pass Outer Bar Channel	47	600-700	28
Aransas Pass Jetty Channel	45-47	600	1.3
Inner Basin at Harbor Island	45	600-1559	0.6
Lower Bay Reach			
Inner Basin Main Channel	45	600	0.6
Humble Basin to Junction at La Quinta Channel	45	500-600	10

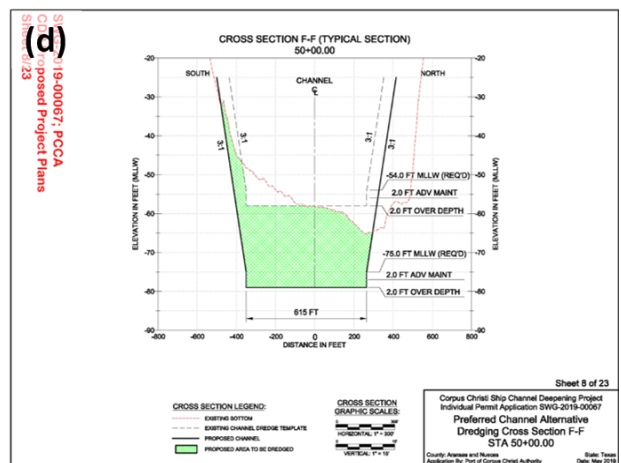
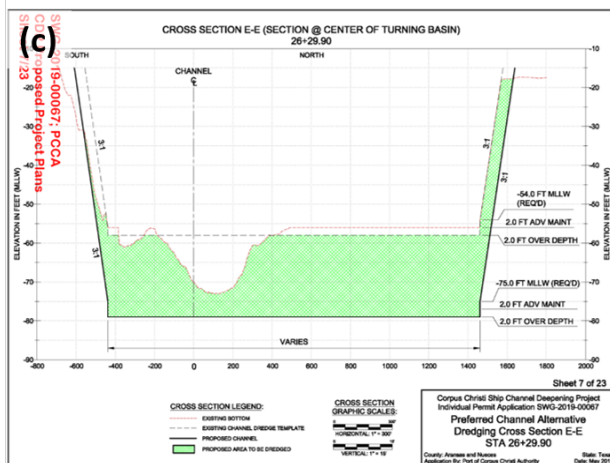
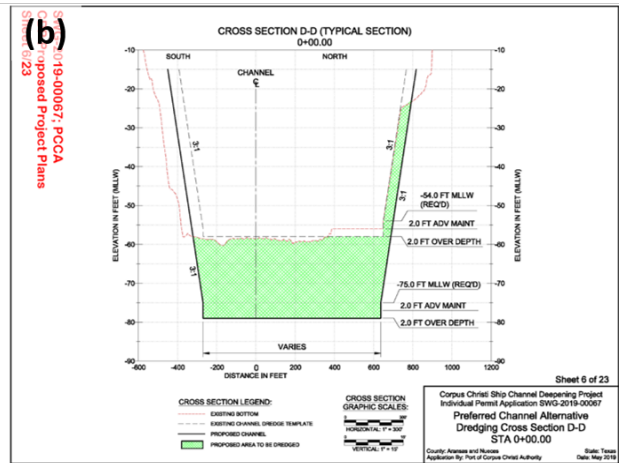
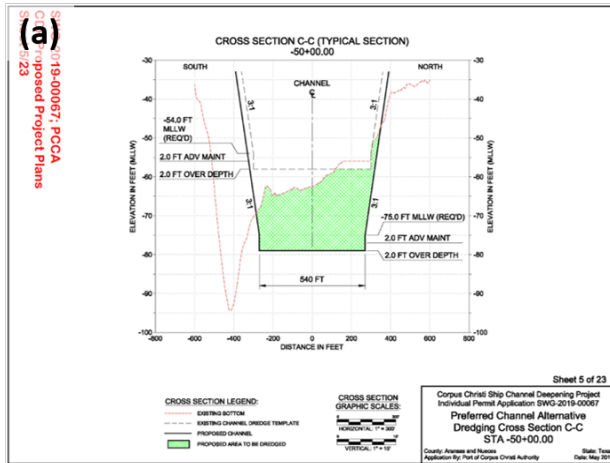


Figure 2-7. Present and planned dredging cross sections for the CCSC in the ferry area. The current bed positions (red, dashed lines) in the study segments generally comply with the existing 54' depth dredge template (gray, dashed lines), whereas the proposed 78' depth plan will implement deeper profiles (thick, solid line). The cross section locations selected for display are denoted in Figure 1-1 and Figure 1-2. (Source: AECOM, 2019).

Panel (d) of Figure 2-7 depicts the channel cross-section closest to the ferry location (F-F). It is worth noting that the existing bottom outline indicates a strong gradient in bed level slope across the channel (red dashed line). At the south bank of the channel, the existing bottom location is 45 feet below MLLW, whereas the north bank features a bottom location of 65 feet below MLLW. Such cross-slope bed level gradients are typical for channel bends. The change in primary flow direction creates a small setup in water level at the outer bank (north bank along Harbor Island in this case) and a corresponding setdown at the inner bank. This small difference in water level elevation is enough to induce a secondary flow cell in the cross-sectional plane analogous to a clockwise current. At the surface, this secondary current flows toward the north bank, while near the bed it flows toward the south bank, continuously scouring sediment at the north edge of the channel and depositing it along the south edge.

Sediment composition of the bed in the vicinity of the ferry terminals is available from various field-sampling campaigns commissioned by the USACE in preparation of channel dredging projects.

Sampling location 3ST-136 (Lat: 27.84, Lon: -97.07) is situated half way between the CCSC centerline and the northern ferry terminal. The Texas Sediment Geodatabase (GLO, 2020) provides access to a sediment core record collected in 1971 (Figure 2-8). The most recent core sample at the same location is from 2018. Both records indicate that the sediments are mainly inorganic sandy or silty clays (CL/ML), clayey sands (SC), and silty sands (SM) with the surface sediments trending toward the finer classifications. SM and SC means more than 50% by weight are retained on the No. 200 sieve (0.075 mm), more than 50% of the coarse fraction pass the No. 4 sieve (4.75 mm), and more than 12% fines by weight are present. For the CL and ML designations, 50% or more by weight are passing the No. 200 sieve and the liquid limit (LL) is less than 50. The actual sediment composition from the 1971 sieve analysis of core materials shows gray silty clay (top 6 feet), gray silty sand (next 8 feet, 64% sand, 36% fines) with shell fragments present in the last 2 feet (2% gravel, 66% sand, 32% fines). The corresponding boring log is presented in the Appendix. An assumed range for a representative median grain diameter of the core material, D_{50} , is 0.02 – 0.2 mm, based on the available sediment data.

In addition to the sediment cores described above, surface sediment grab samples were collected at the same location in 2014. These data were provided by USACE and show a poorly-graded quartz sand (SP) with some small shell fragments and traces of silt and clay. The D_{50} was determined from sieve analysis to be 0.24 mm. It is possible that surface sediments are coarser than core sediments. The exposed surface sediments are usually representative of the hydrodynamic regime at the site and may have been collected at a location where current forces have washed out most fines.

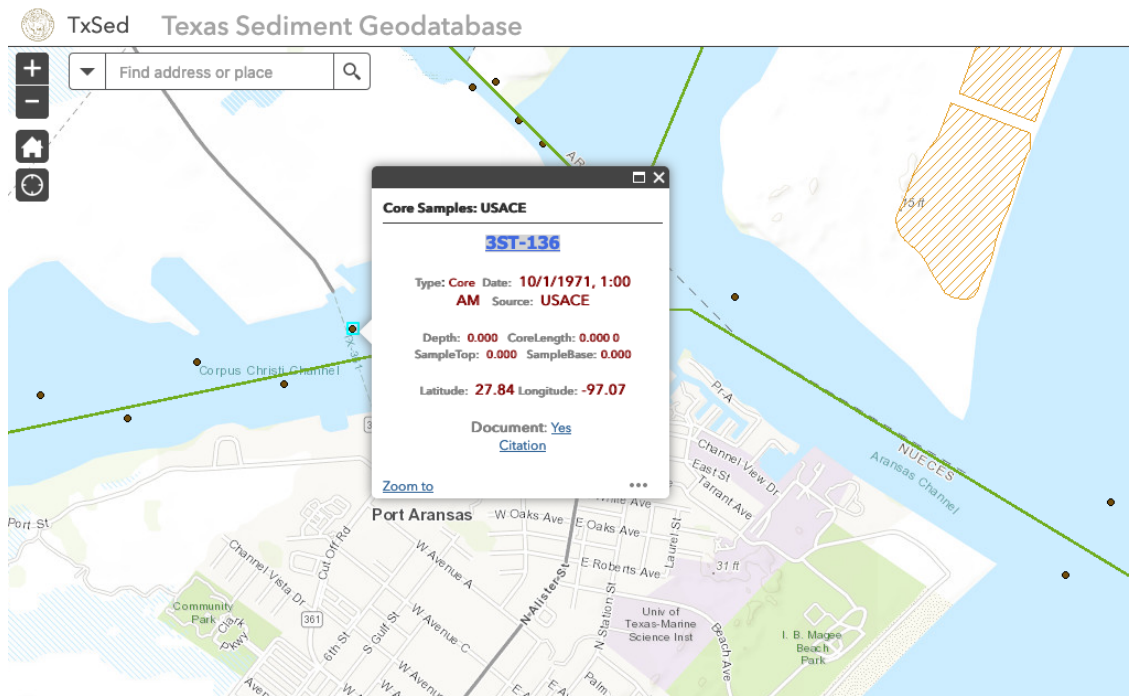
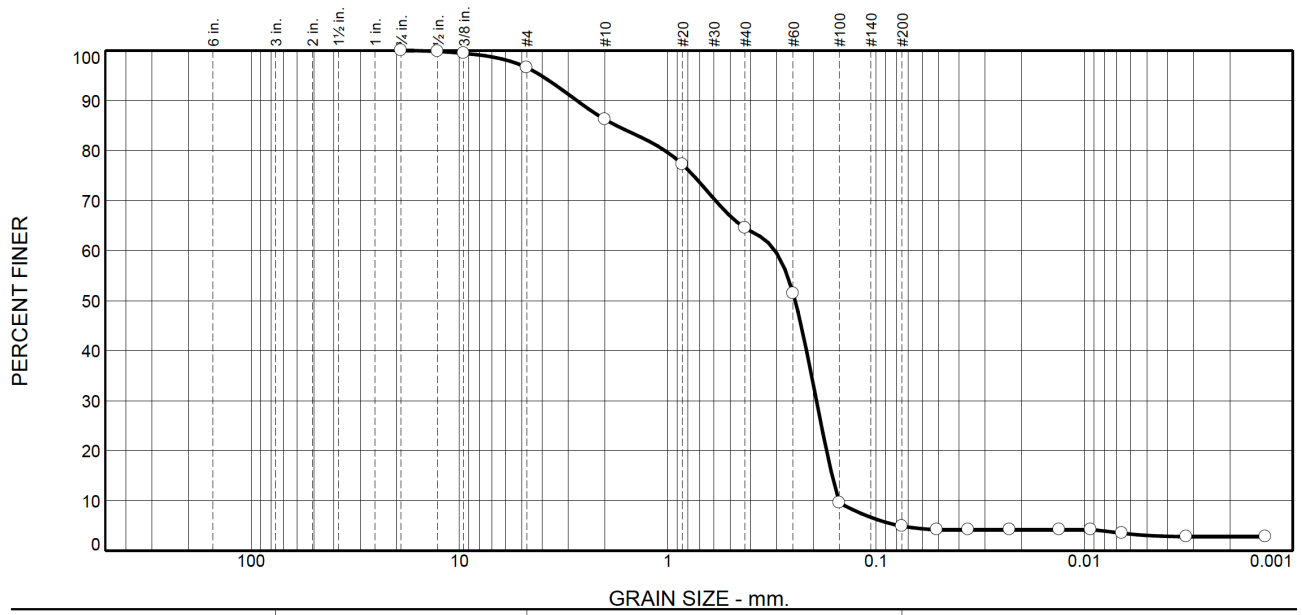


Figure 2-8. Map showing USACE sediment-core sample location 3ST-136.



% +3"	% Gravel		% Sand			% Fines	
	Coarse	Fine	Coarse	Medium	Fine	Silt	Clay
0.0	0.0	3.4	10.4	21.7	59.6	1.8	3.1

Figure 2-9. Grain size distribution of surface grab sample in the CCSC at the ferry location (source: USACE).

3. IMPACT EVALUATION

3.1. Hydrodynamics in Navigation Channels

3.1.1. Hydrodynamic Impact of Channel Modifications

Channel modifications such as deepening and widening can alter the hydrodynamic conditions in the ship channel (i.e., current velocities, wave heights, water elevations) and can affect the degree of bed erosion. Lin et al. (2019) estimated water surface elevation, current velocity, and wave height for the CCCIP 54-foot deepening project using the U.S. Army Engineer Research and Development Center Coastal Modeling System (USACE CMS; Demirbilek and Rosati, 2011). Forcing conditions included typical seasonal wind waves from the south and Hurricane Harvey in 2017. A 50-year sea level rise (SLR) scenario was applied by specifying the projected water level for 2074 as the present water level (2017-2018) + 0.573 m. The model predicted that impacts of the channel modification on the combined water levels and waves at the ferry location were minimal (< 0.04 m). The change of the current velocities was more apparent (0.02 m/s decrease) at the junction of the CCSC and the La Quinta Channel and at the offshore end of the jettied entrance. During April and December 2017, under strong winds, currents reached nearly 1 m/s at the jettied entrance to the CCSC. Currents along the interior of the CCSC increased by 0.1 to 0.2 m/s with the approved 54-foot channel deepening. The difference between mean and maximum wave heights along the CCSC is more significant near the Gulf entrance than in the bay system. Considering a 50-year SLR scenario, currents up to 0.15 m/s stronger (i.e., 5 to 10 percent stronger than without SLR) were produced, especially under high wind and wave conditions. While the changes inside Corpus Christi Bay area were discernible, waves including SLR increased much more in the landlocked portion of the channel in the lower reach area (i.e., in the Humble Basin), where maximum wave heights accounting for SLR were about 0.12 m greater during Hurricane Harvey.

3.1.2. Empirical Equations for Deep Draft Vessel Hydrodynamics

The primary hydraulic forcing on the bank and bottom of the ship channel stems from currents, waves, ship wakes, propeller wash, and drawdown effects that can occur individually or as combinations. Turbulent currents are of particular concern for bed erosion and scour. Highly turbulent currents can occur in the propeller wash or in the return flows due to vessel movement (BAW, 2011). Waves on waterways are generated by either vessel movement (i.e. wakes) or strong winds. Ship-induced wakes are divided into a primary wave system and secondary waves as illustrated in Figure 3-1. The primary wave system includes drawdown, which occurs in the vicinity of a vessel and moves at the same speed. Secondary waves can travel a long way from the vessel similar to free waves. Ship-induced secondary waves are generally considered deep-water waves and the primary wave due to drawdown as a shallow water wave. Rapid changes in water level lead to rapid pore-water pressure changes in the underlying sediments. Particularly, the reduction in external hydrostatic pressure during a vessel drawdown event may increase the pore pressure and force pore water from the subsoil. The loosened soil layer is then susceptible to erosion under the influence of currents, waves, and turbulence. Waves over a sloping bottom increase in steepness (ratio of wave height to wave length) and may eventually break by plunging on the inclined waterway surface producing scour effects as well as run-up and run-down (swash motion). Run-up and run-down flows produce highly erosive conditions generating excess pore-water pressure in the subsoil, further reducing the shear strength and hence stability of the bank.

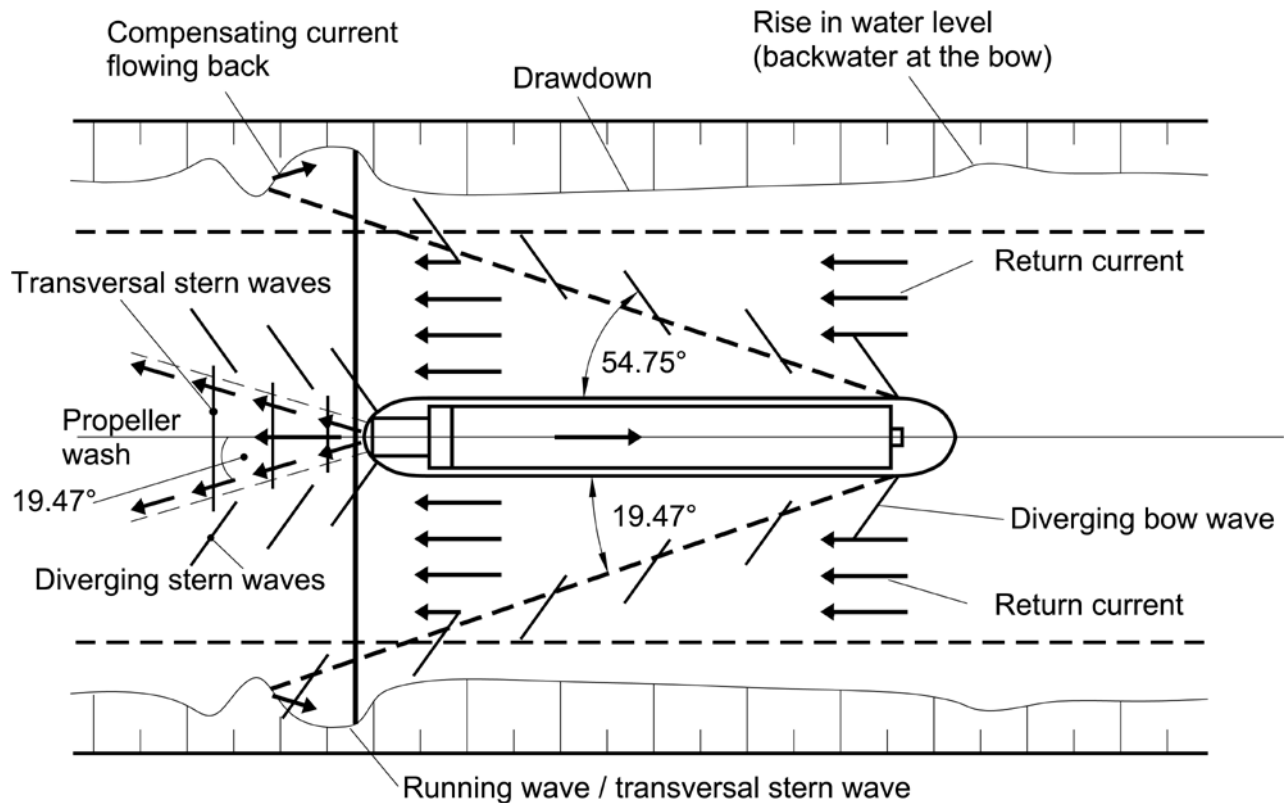


Figure 3-1. Deformation of the water surface (top view) induced by a vessel navigating from left to right in a confined channel (BAW, 2011).

Ships moving in a restricted waterway can generate primary (drawdown) and secondary (transverse and divergent) waves (Bertram, 2012) as illustrated in Figure 3-1 and Figure 3-3. Drawdown is the lowering of the water level adjacent to a vessel caused by the displacement flow. To ensure the geotechnical stability of the channel bed profile, the pore water in the underlying soil needs to be able to follow the changes in water level without significant excess pressures being generated. The secondary waves generated by a ship moving through the water consist of transverse and divergent waves (Bertram, 2012) that often cause adverse impact to adjacent shores. The divergent waves propagate at an angle θ from the centerline of travel and are dependent on hull form (prismatic coefficient), angle of entry, and vessel speed to length ratio. The transverse waves form at the stern, perpendicular to the centerline of travel. The divergent waves can develop significant height and energy, particularly at low or intermediate speeds. The transverse waveform is usually negligible at low speeds but increases with speed up to a length Froude Number of about 0.6. At higher speeds the transverse wave disappears in the range of $0.6 \leq F_L \leq 1.0$ (BAW, 2011; FitzGerald et al., 2011; Ghani and Rahim, 2008).

Drawdown

The maximum drawdown $\Delta \bar{h}$ in the narrowest flow cross-section ($b_s = 530'$ at the section EE') can be calculated by solving Bernoulli's equation together with the continuity equation. The ship speed v_s

can be used to compute $\Delta\bar{h}$ via (BAW, 2011)

$$\Delta\bar{h} = \left[\alpha_1 \left(\frac{\Delta A}{A_c - \Delta A} \right)^2 - 1 \right] \frac{v_s^2}{2g} \quad (3-1)$$

where ΔA defines the reduction in the unmodified channel cross-section A_c (ft² or m²) due to vessel blockage and drawdown and v_s is the ship speed through water (m/s). $\Delta A = A_M + b_m \Delta\bar{h}$. A_M is the submerged mid-ship section calculated as $A_M = BT$. The parameter b_m is the mean channel width at water level in the drawdown area. The parameter b_m is calculated with respect to the channel width at the water level b_{ws} as $b_m = b_{ws} - m \cdot \Delta\bar{h}$ (ft or m) with the mean drawdown depth $\Delta\bar{h}$ (ft or m) and the side slope inclination m (horizontal to vertical). Alternatively, when the width of the channel at the bottom b_s (i.e., the narrowest width of the flow cross section) is known, $b_m = b_s + m \cdot (d - \Delta\bar{h})$. Figure 3-2 illustrates the geometric parameters defining the channel cross-sectional area relative to the mean water surface position.

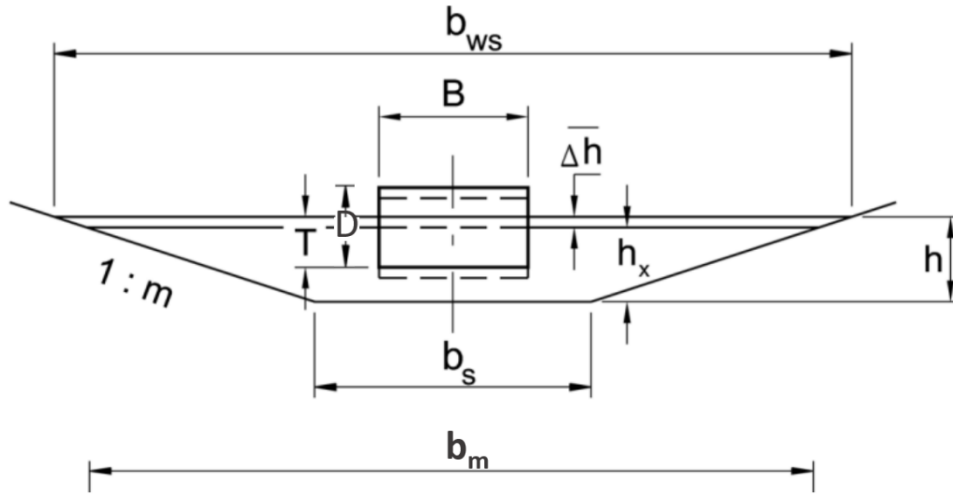


Figure 3-2. Definition sketch for the channel cross-section with respect to the mean water depth (BAW, 2011).

A correction coefficient α_1 accounts for the influence of irregularity of the return flow depending on how close v_s is to the critical ship speed, v_{cr} . The parameter α_1 is calculated as

$$\alpha_1 = 1.4 - 0.4 \frac{v_s}{v_{cr}} \quad (3-2)$$

The critical speed, v_{cr} , is the upper limit of maximum velocity for a disturbance propagating at the free surface of unrestricted shallow water with depth h . The variable v_{cr} is calculated based on the blockage coefficient K_C (Eloot et al., 2008; PIANC, 2014) as

$$v_{cr} = K_C \sqrt{gh} \quad (3-3)$$

$$K_c = \left[2 \sin \left(\frac{\sin^{-1}(1 - C_{bl})}{3} \right) \right]^{1.5} \quad (3-4)$$

where the blockage ratio C_{bl} measures the fraction of the channel cross-sectional area A_c that is blocked by the ship's underwater midship cross-sectional area A_M .

Most significant forces on channel banks due to vessel motion occur in confined channels. The blockage ratio C_{bl} can be used to assess whether a channel can be considered “confined”. C_{bl} may vary from 0.3 to 0.5 for very restricted narrow canals and reduce to 0.05 or below in open channel situations. While there is no accepted limit, depending on ship speed, a blockage ratio greater than 0.05 - 0.1 may lead to ship effects typically seen in confined channels (Maynard, 2004). If a VLCC of assumed dimensions (Section 1.3.1) travels through cross-section F-F (Figure 2-7d) dredged to 79 feet below MLLW, the blockage ratio C_{bl} approaches 0.3.

Finally, the calculation for the maximum drawdown $\Delta \bar{h}$ is performed iteratively after assuming an initial value for $\Delta \bar{h}$ in Equation (3-1) until the calculated speed v_s corresponds to the design ship speed.

The rate of drawdown v_{za} (m/s) by wind or ship-induced secondary waves can be calculated as (BAW, 2011, 2005)

$$v_{za} = \pi H / T_\lambda \quad (3-5)$$

with the wave period T_λ (s) and wave height H (m). The drawdown time is defined as $t_a = T_\lambda / 2$ (s).

Figure 3-3 shows an example of a water level time series for a 15-min period after the passing of a large ferry (L200 x B30 x T7 m) measured at a low wind and low swell site at the Furusund fairway in Sweden (Almström et al., 2014). Each sequence was filtered with a low-pass filter and the drawdown depth due to the primary waves is determined as the minimum water elevation below the mean water level ($z = 0$) after passage of the vessel ($t = 0$). The wave period T_λ (s) is measured as the time interval between two consecutive zero up-crossing points in the water level time series. The wave height H is the vertical distance from the crest to the trough during the period T_λ .

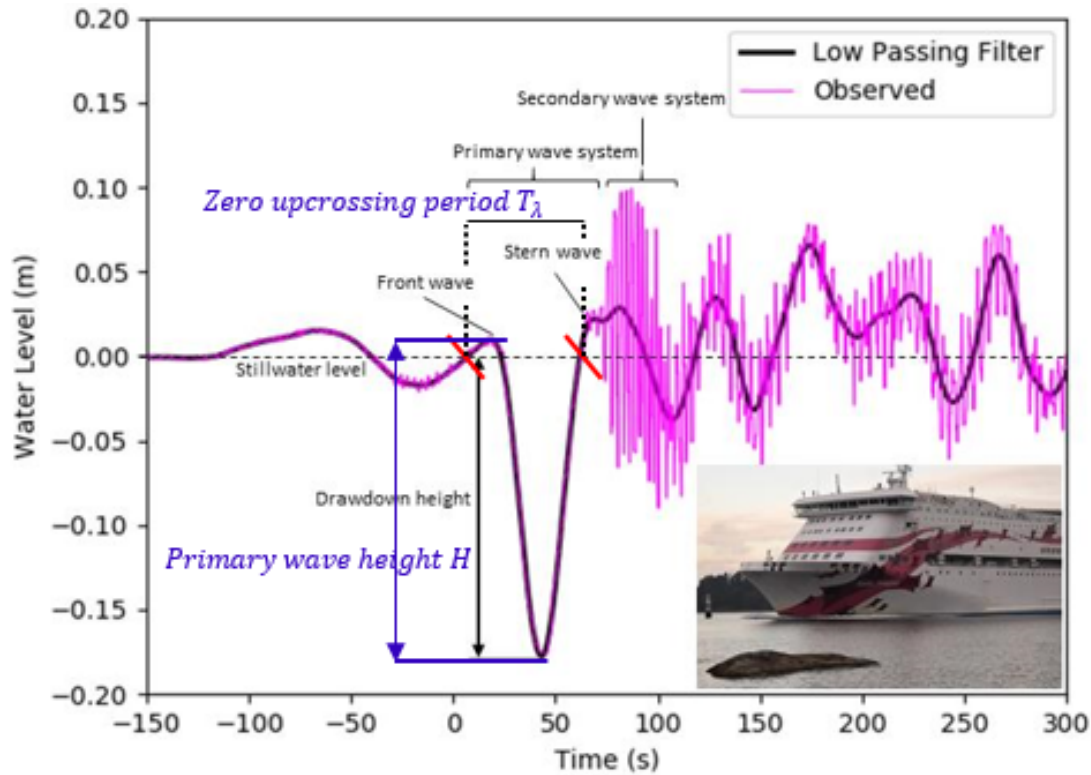


Figure 3-3. Measured water level time series of ship generated waves created by the passenger ferry Baltic Princess. Modified from Figure 1 of Almström et al., (2014).

Return Flow Velocity

The flow around a ship and its wave formation are subject to changes in restricted cross-sections when the ship speed increases. The water volume displaced by the ship moves in the opposite direction of ship movement in the vicinity and starts developing unsteady flows when the critical ship speed has been reached. The one-dimensional calculation of return flow velocity and drawdown can be made based on Bernoulli's equation (integrated linear momentum equation) and the continuity equation (conservation of mass) for a vessel sailing at navigational speed v_s along a canal. The return flow velocity averaged over the cross section \bar{v}_r [m/s] can be calculated as (BAW, 2005)

$$\bar{v}_r = \frac{\Delta A}{A_c - \Delta A} v_s \quad (3-6)$$

Maximum Secondary Ship Wave Height

Maximum wave heights H_m form along the "Cusp Locus" or "Interference" line where transverse and diverging waves meet with the initial angle $\alpha = 19.46^\circ$ relative to the sailing line. H_m varies with the ship speed v_s , distance from the sailing line y , water depth d , and the hull form C_b . The angle of wave front β affects the direction of the energy propagation and the wave length (L) and wave period (T) (Ghani and Rahim, 2008).

C_b is the block coefficient calculated as $C_b = \nabla / (L \cdot B \cdot T)$ with displacement (i.e., immersed

volume) of the ship ∇ . Values of ∇ and C_b are dependent on shape, dimensions, and loading conditions (i.e., percentage of the full capacity) of the vessel. Typical values of C_b are presented in Table 3-1 (Cult of Sea, 2018).

Table 3-1. Typical values of C_b at fully loaded drafts (Cult of Sea, 2018).

Ship Type	Typical C_b Fully Loaded	Ship Type	Typical C_b Fully Loaded
ULCC	0.850	General cargo ship	0.700
Supertanker	0.825	Passenger liner	0.575–0.625
Oil tanker	0.800	Container ship	0.575
Bulk carrier	0.775–0.825	Coastal tug	0.500

Medium-form ships (C_b approx. 0.700), full-form ships ($C_b > 0.700$), fine-form ships ($C_b < 0.700$).

The following equation can be applied to calculate the maximum wave height of the diverging secondary waves at the “locus” points (BAW, 2011; Blaauw, 1984):

$$H_m = C_S \frac{v_s^{8/3}}{g^{4/3} y^{1/3}} f_{cr} \quad (3-7)$$

where C_S (-) is the coefficient dependent on the shape and dimensions of the ship, draft and water depth, and y is the distance from the ship’s side to the bank line (m). Approximated values for C_S are suggested as $C_S = 0.25$ for conventional inland navigation vessels and tugs, 0.35 for empty, single-line push tow units, and 0.80 for fully laden, multi-line push tow units and recreational craft. The coefficient of velocity f_{cr} (-) accounts for the increase in the height of the secondary waves near the critical ship speed and is estimated as

$$f_{cr} = \begin{cases} 1.0 + 0.7 \left\{ \sin \left[\frac{2\pi}{0.8} \left(\frac{v_s}{v_{cr}} - 0.8 \right) \right] \right\}^2 & \text{for } 0.8 \leq \frac{v_s}{v_{cr}} \leq 1.2 \\ 1.0 & \text{otherwise} \end{cases} \quad (3-8)$$

with f_{cr} varying from 1.0 to 1.7.

3.1.3. Propeller Wash

Heavy vessel traffic accompanied by an increase in engine power can produce efflux velocity of a rotating propeller that can be significant in areas of restricted depth and width where the distance between the vessel and the bank is small (of the order of a few hundred meters). Impacts of propeller jets recorded in the literature include: bank and shoreline erosion, vegetation damage, adverse effects on biota, motions of moored vessels, increased stress on fixed and floating structures, changes in beach morphology, and landslides (FitzGerald et al., 2011; Parnell and Kofoed-Hansen, 2001). Ship-induced sediment transport results directly from the propeller current and indirectly from return currents and ship-induced waves. The largest return flow velocities and secondary wave heights occur in the case of a single ship sailing alone close to the bank at a temporarily much faster speed. A vessel casting off with a powerful engine and a large diameter propeller can exert a critical load on banks for a short time while remaining in a static, Ballard thrust condition, position (BAW, 2005).

Efflux Velocity

The decisive parameter for the jet induction is the initial axial velocity or efflux velocity v_0 . The water leaves the propeller with this current velocity. The variable v_0 is the maximum velocity at the face of the propeller (Söhngen and Kayser, 2010) located in the axial direction at a distance of $D_p/2$ behind the propeller axis. The maximum initial axial velocity v_0 calculated for a ship speed through water is zero ($v_s = 0$) based on simplified momentum theory as:

$$v_0 = 1.6f_n n_p D_p \sqrt{K_T} \quad \text{for unducted propellers} \quad (3-9)$$

$$v_0 = 1.6\sqrt{0.5}f_n n_p D \sqrt{K_T} \quad \text{for ducted propellers} \quad (3-10)$$

where D_p is the diameter of the propeller [m or ft], f_n is the propeller rotation factor [-], K_T is the thrust coefficient of the propeller when $v_s = 0$, and n_p is the design propeller rotation rate [1/s]. K_T is estimated as the upper limit for an unducted propeller when $v_s = 0$ as

$$K_T = 0.55 \frac{P}{D_p} \quad \text{for} \quad \left\{ 0 < \frac{P}{D_p} < 1.4 \right\} \quad (3-11)$$

and for a ducted propeller as

$$K_T = 0.67 \frac{P}{D_p} \quad \text{for} \quad \left\{ 0 < \frac{P}{D_p} < 1.8 \right\} \quad (3-12)$$

with the design pitch ratio P/D [-]. $P/D \approx 0.7$ for inland navigation vessels, and ≈ 1.0 for drive pusher craft and bow thruster. The drive pusher vessels are mounted with propeller(s) behind the engine(s). Bow thrusters have the propulsion device(s) mounted to the bow of a ship (Faltinsen, 1990). The suggested values for K_T and f_n are provided in BAW (2005) and DGGT (2012). For example, $f_n \approx 0.75$ for a starting maneuver from a stationary position, and $0.25 \leq K_T \leq 0.50$ for unducted propellers when $v_s = 0$.

The parameter v_0 increases to v_{0J} as the ship gathers speed ($v_s \neq 0$). A practical approximation for the range of v_{0J} can be obtained for unducted propellers as:

$$v_{0J} = v_0 - \frac{1}{3}v_A \quad (3-13)$$

For unducted propellers the value of v_{0J} initially decreases slightly and then increases again. For ducted propellers, the approximation can be obtained as:

$$v_{0J} = v_0 + \frac{1}{3} \frac{v_A^2}{v_0} v_{0J} = v_0 - \frac{1}{3}v_A \quad (3-14)$$

The parameter v_{0J} includes the proportion of the approach flow velocity v_A (= speed v_s from the perspective of an observer moving with the ship).

Main Velocity $v_{x,max}$

The jet reaches the maximum main velocity, $v_{x,max}$, on the jet axis at a distance x from the propeller plane. The decrease in the main velocity is calculated with reference to the initial v_0 and as a function of the relative axial distance behind the propeller x/D_p . The area behind the propeller x/D_p can be divided into three sections: an approach area ($x/D_p \leq 2.6$), and areas where the jet dispersion is unobstructed ($2.6 < x/D_p \leq x_{gr}/D_p$) and obstructed $x_{gr}/D_p < x/D_p$, respectively, by water level, bed or any lateral boundaries.

The main velocity (m/s) in the respective areas behind the propeller plane is calculated for all standard situations as

$$\frac{v_{x,max}}{v_0} = \begin{cases} 1 & \frac{x}{D_p} \leq 2.6 \\ 2.6 \left(\frac{x}{D_p}\right)^{-1} & \text{for } 2.6 < \frac{x}{D_p} \leq \frac{x_{gr}}{D_p} \\ A \left(\frac{x}{D_p}\right)^{-a} & \frac{x_{gr}}{D_p} < \frac{x}{D_p} \end{cases} \quad (3-15)$$

where D_p (m) is the diameter of the propeller. The parameters a and A are quantities depending on the jet dispersion field, the design of the stern of the vessel and the propeller/rudder configuration. Standard approximations for a and A are reported as $0.6 \leq a \leq 1.62$ and $0.8 \leq A < 2.0$ (BAW, 2011) for a propeller without a middle rudder behind it and where the jet dispersion is not restricted by any lateral obstacles.

The distance x_{gr} (m) beyond which the dispersion of the jet is influenced by the channel bed is calculated as

$$\frac{x_{gr}}{D_p} = \left(\frac{A}{2.6}\right)^{1/(a-1)} \quad (3-16)$$

Note that for ship speeds $v_S > 0$, v_{0J} must be used in place of v_0 as a reference velocity.

Jet Velocity Orthogonal to the Jet Axis v_{xr}

The distribution of the jet velocity v_{xr} orthogonal to the jet axis in the area of jet impact is governed by the position of the jet axis above the bed level, h_p at a distance x from the propeller plane. The radial velocity distribution is computed as

$$\frac{v_{xr}}{v_{x,max}} = e^{-22.2(r_x/x)^2} \quad (3-17)$$

Here, r_x is the radial distance of a point considered (e.g., the bed) from the jet main axis at a distance x downstream of the plane of the propeller (m or ft). Figure 3-4 is a schematic illustrating the jet velocity orthogonal to the main velocity axis (e.g., x -axis).

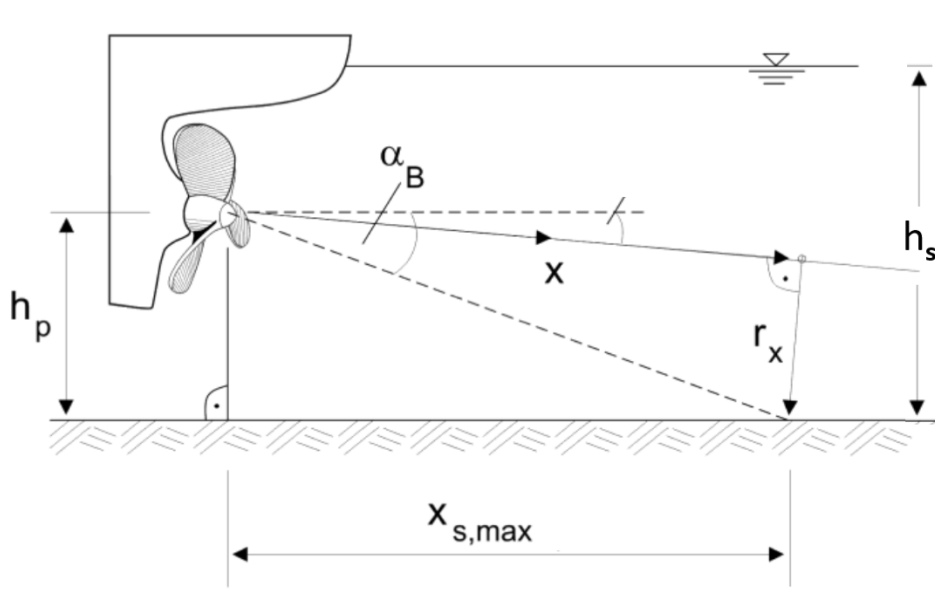


Figure 3-4. Schematic illustration of the parameters used to compute the distribution of near-bed flow velocities orthogonal to the jet axis (BAW, 2005).

Maximum Near-bed Velocity

Equation (3-18) can be used to calculate the maximum near-bed flow velocity $x_{s,max}$. The axial distance of this maximum near bed velocity from the propeller plane $x_{s,max}$ is approximated as

$$x_{s,max} = \frac{h_p}{\tan \alpha_B} \quad (3-18)$$

where h_p is the height of the propeller axis above the bed (m or ft) and α_B is the mean angle of diversion as illustrated in Figure 3-4. The parameter $\alpha_B = 8.5^\circ$ can be used for jet flows that are not restricted laterally.

Simplified equations for the maximum near-bed velocity are presented for propeller advance ratios $v_s = 0$ and $v_s \neq 0$. The maximum near-bed velocity at the point of impact of the propeller jet $v_{b,max}$ can be estimated for $v_s = 0$ as

$$v_{b,max} = E \left(\frac{D_p}{h_p} \right) v_o \quad (3-19)$$

where E is the coefficient for characterization of stern shape and rudder configuration. $E = 0.71$ for slender sterns with a middle rudder, $E = 0.42$ for slender sterns without a middle rudder, and $E = 0.25$ for modern inland navigation craft with a tunnel stern and twin rudders.

When a ship casts off with $v_s > 0$, the induced initial velocity relative to the bed and bank will decrease at the rate at which the propeller jet strikes the boundaries of the waterway. The maximum near-bed velocity $v_{bj,max}$ for a vessel speeding at v_s can be calculated approximately as:

$$v_{bJ,max} = v_{b,max} \left(1 - \frac{v_s}{v_{oJ}} \right) \quad (3-20)$$

3.2. Quantification of Vessel Induced Hydrodynamics

3.2.1. Assumptions and Limitations

The potential values for maximum drawdown, return current, and secondary ship-induced wave heights are calculated using the equations and models presented in Section 3.1.2. The following important simplifications are implemented in the calculation (BAW, 2011) to make such empirical approximations possible:

- a constant drawdown over the length of the vessel
- drawdown at the bow and at the stern are the same
- a constant return flow velocity over the channel cross section
- a frictionless flow

The following complications are not considered in these calculations. They would require a more detailed numerical model study to be included. For a first-order approximation of the situation, however, they can be omitted:

- Shallow water conditions in wide canals or vessels that are short in length relative to the canal width
- Inclination of the water surface between bow and stern.
- Eccentricity of sailing line within the channel.
- Vessel shape and dynamic trim.

3.2.2. Waves Produced by VLCC Motion

The maximum drawdown, return current velocity, and diverging secondary wave height are calculated based on the theoretical models for the vessel dynamics parameters presented in Section 3.1.2. The assumption of a VLCC traveling past the ferry terminals is made to investigate the worst-case scenario possible in light of future VLCC terminal construction upstream of the ferry landings. A reference value for the critical ship speed estimated is also provided. Table 3-2 presents values for the VLCC vessel and navigation channel geometry parameters used in the calculation.

Table 3-2 Model navigation vessel and channel parameter values.

L/B/T (ft/ft/ft)	v_s (knots)	D_p (ft)	C_b (-)	Rated Power, P (SHP)	d (ft, MLLW)	Longitudinal Channel Extent, l (ft)	m (H/V)
1088/228/74	11	31.5	0.84	45,000	79	8000	3

The bottom width of the channel at 79 feet below MLLW varied from 530 to 615 ft between the cross-

section location EE' and FF' (Figure 1-1), along approximately $l = 8,000$ ft longitudinal channel distance (Port of Corpus Christi Authority, 2018). A simple, channel cross-section profile is assumed as shown in Figure 3-5 for the ship-induced wave impact evaluation. Transit speeds from 5 to 10 knots are the most common ship speed in typical harbor channels as observed on a number of projects. A typical tanker designed to achieve 15 to 16 knots (7.7 to 8.2 m/sec (25.2 to 26.9 ft/sec)) in the open ocean would sail at about 11 knots (5.6 m/sec or 18.5 ft/sec) in shallow water (USACE, 2006). Therefore, the sailing speed $v_s = 11$ knots (16.9 ft/s) was applied.

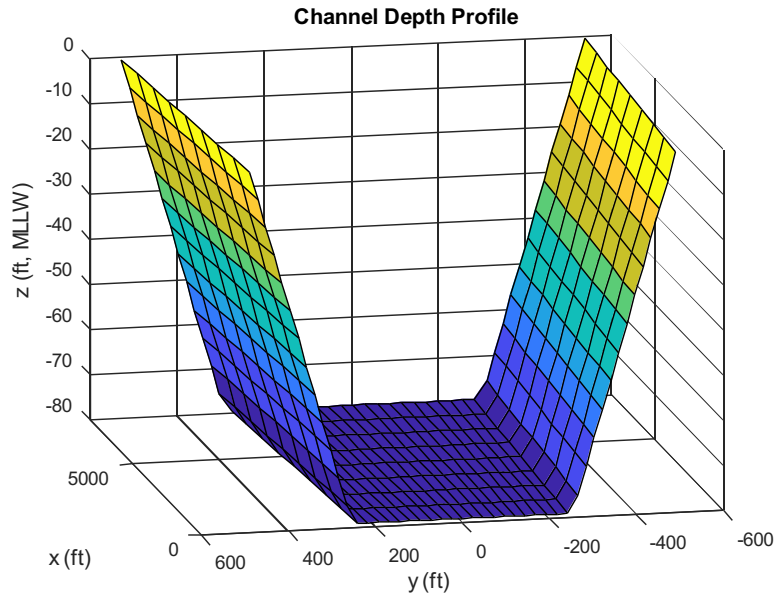


Figure 3-5. Simplified 79-ft depth (MLLW) profile between the cross-section location EE' and FF' shown in Figure 1-1. The bottom width varied from 530 to 615 ft along the channel distance $l = 8,000$ ft.

Drawdown

Equation (3-1) is used to calculate the drawdown $\Delta \bar{h}$ produced by the primary ship wave.

Table 3-3. Maximum mean water depth reduction $\Delta \bar{h}$ due to drawdown and associated coefficients evaluated at a longitudinal distance l_x from section E-E'.

l_x (ft)	$\Delta \bar{h}$ (ft)	A_C (ft ²)	ΔA (ft ²)	α_1 (-)
0 (section EE')	9.0	59,645	17,223	1.01
1,000	8.5	60,484	17,228	1.02
2,000	8.0	61,324	17,233	1.02
3,000	7.5	62,163	17,238	1.03
4,000	7.0	63,003	17,243	1.03
5,000	6.6	63,842	17,248	1.03
6,000	6.3	64,681	17,253	1.04
7,000	5.9	65,521	17,257	1.04
8,000 (section FF')	5.6	66,360	17,262	1.04

Return Flow Velocity

Equation (3-6) is used to calculate the maximum mean return flow velocity \bar{v}_r produced due to the displacement volume in the channel by the submerged ship volume and water surface drawdown.

Table 3-4. Maximum average return current and associated coefficients evaluated at a longitudinal distance l_x from the section E-E'.

l_x (ft)	\bar{v}_r (ft/s)	b_m (ft)
0 (section EE')	11.8	740
1,000	11.2	752
2,000	10.7	764
3,000	10.2	776
4,000	9.7	788
5,000	9.2	800
6,000	8.8	812
7,000	8.4	824
8,000 (section FF')	8.0	835

Maximum Secondary Ship Wave Heights H_m

Equation (3-7) is used to calculate the maximum wave height H_m produced by the diverging secondary waves at the “locus” points within the longitudinal channel extent l_x . Table 3-5 presents the maximum wave height H_m and associated coefficients evaluated across the channel.

Table 3-5. Maximum wave height H_m and associated coefficients evaluated for a cross-sectional area A_c located a longitudinal distance l_x from the section E-E' and lateral distance y from the channel centerline.

l_x (ft)	H_m (ft)			C_S (-)	A_c (ft ²)	v_{cr} (ft/s)	f_{cr} (-)
	$y = 0.5B$	$y = 1.0B$	$y = 2.0B$				
0 (section EE')	5.2	2.1	1.4	0.25	59,645	19.3	1.65
1,000	4.6	2.0	1.4	0.25	60,484	19.5	1.61
2,000	4.2	1.9	1.3	0.25	61,324	19.7	1.58
3,000	3.8	1.9	1.3	0.25	62,163	19.9	1.53
4,000	3.5	1.8	1.3	0.25	63,003	20.1	1.49
5,000	3.2	1.7	1.2	0.25	63,842	20.2	1.45
6,000	3.0	1.6	1.2	0.25	64,681	20.4	1.40
7,000	2.8	1.6	1.1	0.25	65,521	20.6	1.36
8,000(section FF')	2.6	1.5	1.1	0.25	66,360	20.8	1.32

The values presented in Table 3-5 clearly show the potential of a VLCC crossing the ferry path to produce vessel-induced waves approaching the critical maximum wave height value of 6 feet (Section 1.3.4).

In summary, the passage of a VLCC vessel can cause ~9.0 ft (2.7 m) water surface depression due to the ship-induced drawdown. The reduced channel cross-sectional area due to displacement by the vessel's underwater section and mean water depth reduction due to primary wave's drawdown can produce return currents that flow near the vessel and in the opposite direction of vessel motion. The return flow velocity averaged over the cross section \bar{v}_r could reach 8.0 – 11.8 ft/s (2.4 – 3.6 m/s) across the varying channel cross-section areas. The diverging secondary ship waves can result in a maximum wave height on either side of the VLCC, that is, as high as 5.2 ft (1.6 m) in the narrow stretch of the ship channel near the ferry system.

3.2.3. Propeller Wash Analysis Results

Even though VLCC's are not self-propelled within the bounds of the CCSC, the potential for propeller wash generated from the tug boats or other vessels crossing the ferry path still exists. Here, an attempt is made to identify potential issues based on empirical equations for propeller wash. The maximum flow velocities associated with the propeller wash are calculated for the hypothetical situation where a vessel starts to maneuver from a stationary position using an unducted propeller with $v_s = 0$. The following design parameters were chosen to characterize the flow during such operations and can be modified based on desired vessel characteristics.

Table 3-6. Design parameters used to calculate propeller-wash flow velocities.

L/B/T (ft/ft/ft)	v_s (knots)	D_p (ft)	C_b (-)	Rated Power, P (HP)	Water depth, d (ft, MLLW)
160/52/5	0	13.4	0.6	670	79

Efflux Velocity

Equation (3-9) is used to calculate the efflux velocity v_0 and the result and associated parameters are presented in Table 3-7.

Table 3-7. Efflux velocity v_0 and associated coefficients.

v_0 (ft/s)	P/D_p (-)	f_n (-)	K_T (-)
16.4	0.7	0.75	0.39

Maximum Main Velocity $v_{x,max}$

The maximum main velocity, $v_{x,max}$, is calculated along the jet axis (i.e., x -axis) using equation (3-15). The parameter $v_{x,max}$ is essentially the variation of v_0 in the shallow water depth h_s over the axial distance x from the propeller plane. The shallow water depth h_s is defined as the water depth below the water line at the draft of a vessel (Figure 3-4). Typical values are $h_s = 1 - 9D_p$ and Figure 3-6 presents the variation of $v_{x,max}$ with $h_s = 3, 6, \text{ and } 9D_p$. The hard channel boundary starts influencing the jet dispersion from a distance x_{gr} behind the propeller surface. The distance x_{gr} tends to increase with water depth h_s as indicated in Figure 3-6 (\times symbols) for the respective h_s cases.

Table 3-8 The maximum main velocity at various shallow water depths.

h_s		x_{xgr}		$v_{x,max}$		A (-)	a (-)
	(ft)		(ft)		(ft/s)		
$3D_p$	14.8	$4.5D_p$	14.8	$0.58v_0$	9.50	1.43	0.6
$6D_p$	29.5	$8.9D_p$	29.5	$0.29v_0$	4.76	1.08	0.6
$9D_p$	58.8	$17.8D_p$	58.8	$0.15v_0$	2.39	0.82	0.6

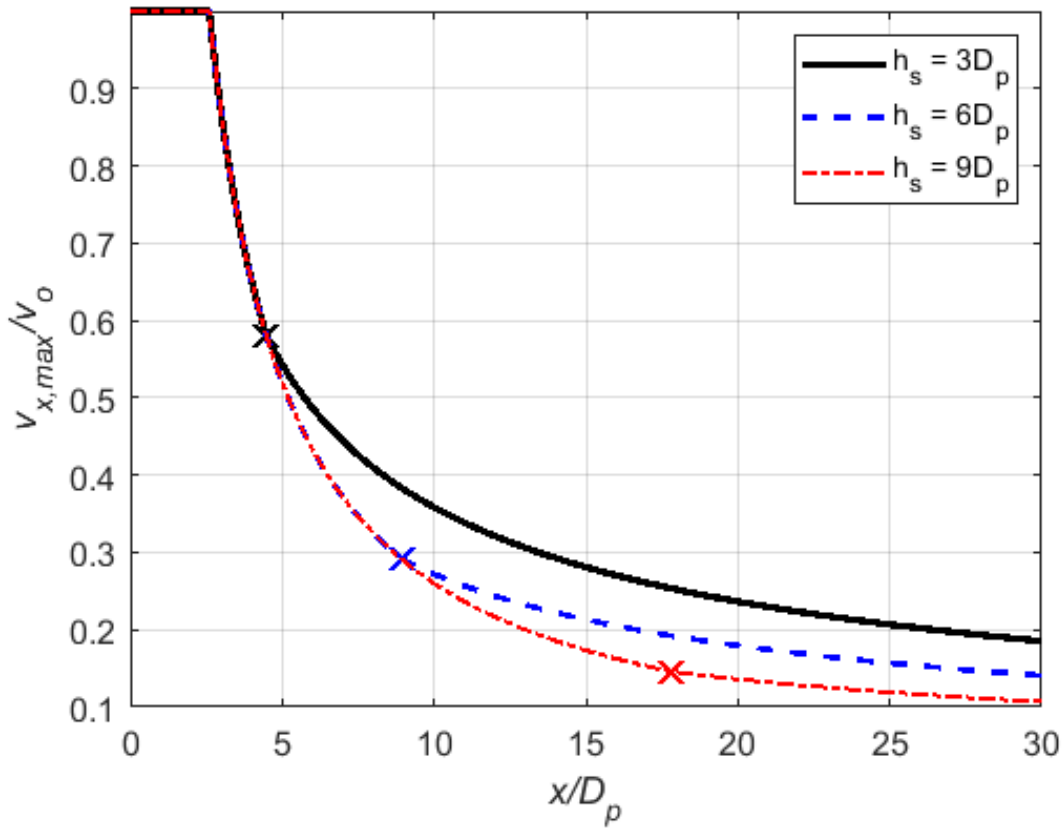


Figure 3-6. Maximum main velocity, $v_{x,max}$, on the jet axis at a distance x from the propeller plane. Velocities and the axial distance are referenced to the efflux velocity v_0 and the design propeller diameter D_p .

Maximum Near-Bed Velocity

The maximum near-bed velocity $v_{b,max}$ at the axial distance $x_{s,max}$ from the propeller plane is calculated using Equations (3-18) and (3-19). Typical values are $h_s = 1.5 - 8D_p$ and Table 3-9 presents values of $x_{s,max}$ and $v_{b,max}$ calculated for $h_p = 1.5, 3, \text{ and } 8D_p$ and $E = 0.42$.

Table 3-9. Maximum near-bed velocities at various water depths below the propeller main axis.

h_p		$x_{S,max}$		$v_{b,max}$		E	α_B
	(ft)	(m)	(ft)		(ft/s)	(-)	(°)
$1.5D_p$	5.0	10.0	33.1	$0.28v_o$	4.6	0.42	8.5
$3D_p$	9.9	20.1	66.2	$0.14v_o$	2.3	0.42	8.5
$8D_p$	26.4	53.5	176.6	$0.05v_o$	0.9	0.42	8.5

3.3. Morphological Changes

Most significant forces on channel banks due to vessel motion occur in confined channels. The ship effects influencing the bank can be categorized as long- or short-period. Long-period effects are comprised of surge, return velocity, drawdown, and transverse stern waves. In this context surge is a relatively small elevation change in water level affecting an area approximately one ship-length ahead of the vessel. It is essentially a bulge of water being pushed by the moving vessel (i.e., piston effect). This surge effect is better known as a bow wave. The return velocity results from the displacement of the vessel causing movement of water from bow to stern. As potential energy changes to kinetic energy adjacent to the ship, water level (“potential energy”) is lowered and the flow velocity (“kinetic energy”) increases. The confined nature of a channel enhances this phenomenon due to the restricted cross-section available for water flow. Drawdown stems from the same physical phenomenon of reduced water levels near a vessel. The depression in the water surface can then propagate from the vessel similar to a shallow water wave. Transverse stern waves are generated as a result of the local flow conditions at the stern of the vessel and are linked to the changes in water level elevation caused by the moving vessel as well. A transverse stern wave is analogous to an open channel hydraulic jump moving along the channel at the speed of the vessel. A hydraulic jump is an abrupt rise in water surface where flow of higher velocity (supercritical flow) meets flow of lower velocity (subcritical flow). These waves usually have the most pronounced effect on banks in confined channels. The entire sequence comprising the bow wave (surge), drawdown, and transverse stern wave are known as the primary wave of a vessel with a length usually corresponding to the ship length.

Short-period effects include secondary waves formed at the bow and stern, propeller jet effects, and short-period undular wakes following the drawdown. The latter waveform can reach significant heights approaching the magnitude of the drawdown in some cases, at which point it will have a significant effect on the bank (Maynard, 2004).

The combined effect of the vessel-induced hydrodynamics and the tidal currents can cause erosion issues along ship channels. While there is no simple formula available to predict erosion due to ship passage, empirical approaches based on critical bed shear stress or the energy required to initiate movement of bottom sediments can give first-order estimates of erosion potential that could ultimately lead to scour issues at the ferry facilities. In a study on ship impacts on confined channels with very similar bed materials present, Larson et al. (2017) found that the hydrodynamics produced by vessel drawdown or secondary waves were the most critical driver for bed erosion. However, secondary ship waves can become just as important as others have reported (i.e., Maynard, 2004).

Mobilization of material at the bed is related to shear stress at the bed. The bed shear stress produced by wave motion can be estimated from the quadratic friction law as

$$\tau_D = 0.5\rho f_w u_D^2 \quad (3-21)$$

with ρ being the water mass density, f_w being the wave friction factor (assumed 0.02 following the discussion in Le Roux, 2003), and u_D being the horizontal velocity at the bed due to drawdown or secondary wave motion.

For granular material (i.e., sand) a first-order estimate of erodability can be obtained using the Shields diagram. If we consider a maximum bed velocity of $u_D = 2.4$ m/s produced by the return flow (due to drawdown or the secondary wave of a VLCC), the corresponding bed shear stress τ_D based on Equation (3-21) can be estimated to be approximately 58 Pa. Using the sediment median diameter $D_{50} = 0.24$ mm (Figure 2-9) from the USACE surface sample, an approximate unit weight of water of 10,000 N/m³, and a specific density of 2.65 for quartz sand, the Shields parameter can be determined as

$$\phi = \frac{\tau_D}{\gamma(S_s - 1)D_{50}} = 14.6 \quad (3-22)$$

which is well above the critical Shields value $\theta_c = 0.04$ (or critical bed velocity $u_c = 0.13$ m/s) for the corresponding grain Reynolds number of 24. This indicates that the granular surface material can definitely be moved by a VLCC based on the assumed parameters.

For mixed and cohesive sediments, the situation becomes more complicated as cohesion, chemical, and even biological parameters can affect erodability in addition to mixture composition and clay type. An empirical relationship for the erosion threshold τ_e (critical shear stress) of mixed sediments including sand, silt, and clay fractions, based on the cohesiveness of the sediment expressed by the plasticity index (PI) of the soil is given by (Smerdon and Beasley, 1959) and has been confirmed by (Jacobs et al., 2011) as

$$\tau_e = 0.163 PI^{0.84} \quad (3-23)$$

where PI is given in percent.

The sandy or silty clay material found in the upper layer of the sediment core sample described in Section 2.3 with a PI of 26 yields an erosion threshold stress of 2.5 Pa based on Equation (3-23). This value is well below the maximum bed shear stress that can be produced by a VLCC, suggesting the potential for erosion. It has to be understood, however, that these potentially erosive conditions would only occur very intermittently and only if a VLCC were to travel past the ferry location (only a future hypothetical scenario with an additional VLCC terminal upstream of ferry operations, not the scenario created by the planned Harbor Island VLCC terminal). More importantly, these conditions are based on first-order empirical equations using worst-case scenario input parameters.

4. FINDINGS AND RECOMMENDATIONS

This study provides a first look at potential impacts on ferry operations from the movement of anticipated Very Large Crude Carrier (VLCC) vessels and Corpus Christi Ship Channel (CCSC) modifications in the vicinity of the TXDOT Port Aransas ferry landings. Findings are based on publicly available documents at the time of the report generation and additional information provided by TXDOT. Furthermore, discussions with personnel from the Port of Corpus Christi Authority (PCCA), AECOM, Mott MacDonald, HDR, and USACE Galveston District (SWG) have helped form the basis for the report.

The analysis reveals that VLCC vessels traversing the ferry path could cause negative impacts to ferry operations as VLCC-produced hydrodynamics such as wakes, drawdown effects, and return flow velocities could reach values on the order of safe ferry operation limits. VLCC drawdown, wake, and return current parameters in combination with ship channel geometry have the potential to cause temporary unsafe ferry operating conditions and extended scour at landing quay walls. This assessment is based on the empirical equation analysis presented in this study and does take into account that VLCCs are being moved via tug boats. If future plans for a VLCC terminal west of the Harbor Island ferry landing were to come to fruition, these potential impacts need to be investigated in further detail.

The current and planned modifications associated with the new VLCC terminal on Harbor Island, directly east of the Harbor Island ferry terminal, should have only minor potential impacts to TXDOT ferry operations and infrastructure. There are two primary reasons for this. For one, the deepening of the ship channel does not create critical increases in currents and wind waves at the ferry site. Secondly, VLCC vessels being maneuvered in and out of the planned Harbor Island terminal do not pass the ferry and are being moved by tug boats rather than being self-propelled.

A circular quay wall is proposed to protect the Harbor Island TXDOT ferry terminal from hydrodynamic impacts due to VLCC and tug boat movement in the new Harbor Island VLCC terminal and to minimize any modifications to existing circulation patterns during peak tide flow. The actual wall design had not been finalized at the time of writing of this report, but several options are under consideration that include an extension of the quay wall toward the ship channel and various levels of perforation (i.e., gaps in the wall) to make the wall semi-permeable to water and sediment flow. While design drawings from publicly available permit applications show the proposed quay wall extending toward the ship channel as far as the existing northern quay wall at the ferry terminal, discussions with PCCA and TXDOT personnel indicated that such a wall could potentially be extended further toward the ship channel, if deemed necessary. An extension (i.e., by 50 feet) could lead to further reduction in current velocity and wake energy reaching the Harbor Island ferry landing, but could also lead to increased sedimentation at the ferry landing. Further design steps to optimize this quay wall need to consider the local effect of perforation, where current speeds are highly increased through the gaps causing heightened potential for local scour at the bed. Reducing flow velocities at the ferry landing site may be beneficial for ferry docking, but can also lead to increased levels of siltation and an increased velocity gradient between the ferry docking area and the open channel that has to be traversed by the ferry vessels. These factors should be considered when finalizing the quay wall design.

In the following, these findings and further thoughts are presented.

VLCC movement impact on ferry operations:

- If an additional VLCC terminal were to be built west of the Ferry landing as mentioned in some of the discussions with TXDOT and other stakeholders, the hydrodynamic forces from VLCC vessels moving past the ferry operations could cause quite significant negative impacts based on performed empirical equation analyses. Due to the large block coefficient of the moving VLCC vessels, a high potential for bank erosion, scour formation, large wake/drawdown, and even ferry vessel downtime exists. The actual impacts will depend on the frequency and motion parameters of VLCC passage but computations with worst-case-scenario values suggest significant issues that require further detailed investigation if plans for such an additional VLCC terminal should move ahead.
- As VLCC vessels entering and leaving the planned VLCC terminal on Harbor Island will be maneuvered by tug boats without passing the ferry landings and without crossing the ferry path, minimal hydrodynamic disturbance of ferry operations is expected.

Quay wall impact on ferry operations:

- The final design of the anticipated circular quay wall between the planned Harbor Island VLCC terminal basin and the northern Ferry terminal needs to be investigated carefully to avoid negative impacts to Ferry operations.
- While an extension of the wall further toward the ship channel could reduce circulation currents at the ferry landing area during peak tide flows, such a configuration may create a situation where larger velocity gradients between the ferry landing area and the open channel exist.
- Introducing gaps into the quay wall to allow for some flow of water and sediment can be used to fine-tune the system but heightened potential for bed scour may exist at these openings due to increased flow velocities.

Channel deepening impacts on ferry operations:

- Wind wave heights are only minimally affected by planned channel deepening efforts in the vicinity of the ferry.
- Currents in the ship channel may slightly decrease due to the channel deepening efforts. These decreases will most likely be offset by future sea level rise.
- The shape of the present cross-section near the ferry suggests secondary current circulation driving bed sediment from the north to the south side of the channel. This will likely continue, even after deepening efforts, and will thus alleviate any potential siltation issues at the Harbor Island ferry landing that could ensue due to an extended circular quay wall.
- The effect of VLCCs passing the ferry landing with the new quay wall need to be investigated further. The potential for VLCC wakes interacting with the wall and the existing ferry docks in an unfavorable manner exists.

Recommendations:

A number of non-public, vessel-passing studies for the area of investigation have been or are being conducted by various entities. TXDOT should discuss with the PCCA and respective consultants the results of these vessel-passing studies in detail as they become available.

Consider discussing with the PCCA the design of the circular bulkhead wall currently given in publicly available permit documents. The implications of an extension of 50 feet toward the channel need to be thoroughly understood. Similarly, the inclusion of gaps in the extended wall needs to be carefully investigated in light of scour potential and increased velocity gradients that would have to be overcome by arriving and leaving ferries.

The empirical analysis on hydrodynamics created by VLCC movement indicates that various potential impacts on ferry operations are possible (i.e., wake, current, scour) in the event that another VLCC terminal is built west of the ferry landings at which point VLCC vessels will traverse past ferry installations. A proactive approach is suggested that should include a numerical model simulation of VLCC vessels passing ferry vessels and landings in various configurations.

5. ACKNOWLEDGEMENTS

This project was funded through Interagency Cooperation Contract (ICC) No. 23868 between the Texas Department of Transportation (Receiving Agency) and the Texas A&M Transportation Institute (Performing Agency).

6. REFERENCES

- AECOM, 2019. Port of Corpus Christi Authority Corpus Christi Ship Channel Deepening Nueces and Aransas Counties, Texas (Project Description for Corpus Christi Ship Channel Deepening Project No. Department of the Army Permit Application SWG-2019-00067). Port of Corpus Christi Authority.
- Almström, B., Larson, M., Granath, L., Hanson, H., 2014. Ship-generated waves over a complex bathymetry. *Coastal Engineering Proceedings (ICCE 2014)*, Seoul, Korea.
- BAW, 2011. Code of Practice Principles for the Design of Bank and Bottom Protection for Inland Waterways (GBB) (BAW Codes of Practice and Guidelines No. Issue 2010). Federal Waterways Engineering and Research Institute, Karlsruhe, Germany.
- BAW, 2005. Principles for the Design of Bank and Bottom Protection for Inland Waterways (Bulletin No. 88). Federal Waterways Engineering and Research Institute (Bundesanstalt für Wasserbau), Karlsruhe, Germany.
- Bertram, V. (Ed.), 2012. Practical Ship Hydrodynamics, in: Practical Ship Hydrodynamics (Second Edition). Butterworth-Heinemann, Oxford, p. iii. <https://doi.org/10.1016/B978-0-08-097150-6.10007-7>

- Blaauw, H.G., 1984. Design of Bank protection of Inland Navigation Fairways, Publication (Waterloopkundig Laboratorium (Delft, Netherlands)) ; no. 320. Delft Hydraulics Laboratory, Delft, The Netherlands.
- Cox, D.T., Hobensack, W., Sukumaran, A., 2017. Bottom stress in the inner surf and swash zone. *Coastal Engineering Proceedings* (ICCE 2000). [https://doi.org/doi:10.1061/40549\(276\)9](https://doi.org/doi:10.1061/40549(276)9)
- Cult of Sea, 2018. Coefficients of Form - Ship's Waterplane, Block, Midship and Prismatic Coefficient. Cult Sea. URL <https://cultofsea.com/ship-stability/coefficients-of-form-ships-waterplane-block-midship-and-prismatic-coefficient/> (accessed 10.16.20).
- Dean, R.G., Dalrymple, R.A., 2001. Coastal Processes with Engineering Applications. Cambridge University Press, Cambridge. <https://doi.org/10.1017/CBO9780511754500>
- Demirbilek, Z., Rosati, J.D., 2011. Verification and Validation of the Coastal Modeling System; Report 1: Summary Report. Engineer Research and Development Center, Coastal Hydraulics Laboratory, U.S. Army Corps of Engineers.
- DGGT, 2012. Water Levels, Water Pressure, Drainage. In: Recommendations of the Committee for Waterfront Structures, Harbours and Waterways. Wiley Online Books, German Society for Geotechnics, pp. 78–105.
- Eloot, K., Verwilligen, J., Vantorre, M., 2008. An Overview of Squat Measurements for Container Ships in Restricted Water. In: Varyani, K. (Ed.), *Safety and Operations in Canals and Waterways, Conference Proceedings*. University of Strathclyde Glasgow & University of Glasgow, pp. 106–116.
- Faltinsen, O.M., 1990. Sea Loads on Ships and Offshore Structures, Cambridge Ocean Technology Series; Cambridge University Press, Cambridge.
- FitzGerald, D., Hughes, Z., Rosen, P., 2011. Boat Wake Impacts and their Role in Shore Erosion Processes, Boston Harbor Islands National Recreation Area (Natural Resource Report No. NPS/NERO/NRR—2011/403). U.S. Department of the Interior National Park Service, Natural Resource Program Center, Fort Collins, Colorado.
- Ghani, M.A., Rahim, M.A., 2008. The prediction of wake wash in the towing tank. *Jurnal Mekanikal*, 26/2.
- GLO, 2020. Texas Coastal Sediment Geodatabase (TxSed) [WWW Document]. Tex. Gen. Land Off. URL <https://cgis.glo.texas.gov/txsed/index.html> (accessed 10.1.20).
- Huthnance, J.M., 1995. Circulation, exchange and water masses at the ocean margin: the role of physical processes at the shelf edge. *Progress in Oceanography* 35, 353–431. [https://doi.org/10.1016/0079-6611\(95\)80003-C](https://doi.org/10.1016/0079-6611(95)80003-C)
- Huthnance, J.M., 1981. Waves and currents near the continental shelf edge. *Progress in Oceanography* 10, 193–226.
- Jacobs, W., Le Hir, P., Van Kesteren, W., Cann, P., 2011. Erosion threshold of sand–mud mixtures. Proc. 9th Int. Conf. Nearshore Estuar. *Cohesive Sediment Transp. Process.* 31, S14–S25. <https://doi.org/10.1016/j.csr.2010.05.012>
- Larson, M., Almström, B., Göransson, G., Hanson, H., Danielsson, P., 2017. Sediment movement induced by ship-generated waves in restricted waterways. In *Coastal Dynamics*, 120, 300–311.

- Le Roux, J.P., 2003. Wave friction factor as related to the Shields parameter for steady currents. *Sedimentary Geology*, 155, 37–43. [https://doi.org/10.1016/S0037-0738\(02\)00157-4](https://doi.org/10.1016/S0037-0738(02)00157-4)
- Lin, L., Demirbilek, Z., Islam, M.S., 2019. Numerical modeling of hydrodynamics and waves for corpus christi ship channel, texas. *E-proceedings of the 38th IAHR World Congress*, Panama City, Panama. <https://doi.org/10.3850/38WC092019-1063>
- Maynard, S., 2004. Ship effects at the bankline of navigation channels. *Proc. Inst. Civ. Eng. - Marit. Eng.* 157, 93–100. <https://doi.org/10.1680/maen.2004.157.2.93>
- NOAA, 2020. National Weather Service Marine Forecasts [WWW Document]. URL <https://www.weather.gov/marine/faq#12> (accessed 10.19.20).
- Parnell, K.E., Kofoed-Hansen, H., 2001. Wakes from large high-speed ferries in confined coastal waters: Management approaches with examples from New Zealand and Denmark. *Coastal Management*, 29, 217–237. <https://doi.org/10.1080/08920750152102044>
- PIANC, 2014. Harbour Approach Channels Design Guidelines, PIANC Report No. 121. Maritime Navigation Commission.
- Port of Corpus Christi Authority, 2018. Corpus Christi Ship Channel Improvement Project.
- Short, A.D., 2012. Coastal Processes and Beaches. *Nat. Educ. Knowl.* 3(10): 15.
- Smerdon, E.T., Beasley, R., 1959. The tractive force theory applied to stability of open channels in cohesive soils. University of Missouri, College of Agriculture, Agricultural Experiment Station.
- Söhngen, B., Kayser, J., 2010. Design of bank and bottom protection. *Hydraul. Eng. Repos. HENRY, On Course - PIANC Magazine* 140 Externe Fachbeiträge.
- TxDOT, 2020. Ferry Information [WWW Document]. Tex. Dep. Transp. State Tex. URL <https://www.txdot.gov/inside-txdot/division/maritime/ferry-schedules.html> (accessed 7.16.20).
- US EPA, 2012. Vessel Safety Manual. Office of Administration and Resources Management Safety. Health and Environmental Management Division, Washington, DC.
- USACE, 2016. Galveston Harbor Channel Extension Feasibility Study Houston-Galveston Navigation Channels, Texas (Feasibility Report). U.S. Army Corps of Engineers, Galveston District Southwestern Division.
- USACE, 2015. MLT to MLLW Vertical Datum Conversion Engineering Design Report: Galveston Harbor, Texas City Ship Channel, Houston Ship Channel. Galveston, TX: Galveston District, Southwestern Division. U. S. Army Corps of Engineers.
- USACE, 2006. Hydraulic Design of Deep-Draft Navigation Projects (Engineer Manual No. EM 1110-2-1613). U.S. Army Corps of Engineers, Washington, DC.
- USACE, 2003. Corpus Christi Ship Channel, Texas Channel Improvement Project Volume 1 (Final Feasibility Report and Final Environmental Impact Statement). U.S. Army Corps of Engineers, Galveston District Southwestern Division.
- Webb, P., 2019. Introduction to oceanography.

Wolanski, E., 2007. Chapter 2 - Estuarine Water Circulation. In: Wolanski, E. (Ed.), *Estuarine Ecohydrology*. Elsevier, Amsterdam, pp. 17–39. <https://doi.org/10.1016/B978-044453066-0.50003-9>

Wood Environment & Infrastructure Solutions, Inc., 2019. Revised Application for a Standard Department of the Army Section 10 and Section 404 Permit (No. 6703180051.0002). Port of Corpus Christi Authority of Nueces County.

7. Appendix

Below, the 1971 boring log for USACE core sample location 3ST-136 between the CCSC centerline and the northern ferry landing is shown:

BORING LOG										Boring No. <u>3ST 136</u> Levee District <u>SALVESTON</u> Job No. <u>1381</u>			
FIELD DATA										LABORATORY DATA			
Project <u>PORT ARANSAS-CORPUS CHRISTI WATERWAY</u> Location <u>INNER BASIN</u>					Surface Elev. _____					Date _____			
Drill Rig <u>ARCO #4</u> Inspector <u>CANNON</u> Operator <u>SMITH</u>					Natural Ground Elev. <u>36.0 MLT</u>					Classified by _____			
SAMPLE NUMBER	DATE TAKEN	STRATUM		DRIVE		SAMPLE		TYPE OF SAMPLER	CONTAINER	CLASSIFICATION AND REMARKS	CLASSIFICATION	SYMBOL	NAT WC %
		FROM	TO	FROM	TO	FROM	TO						
	<u>10 OCT 1971</u>	<u>0.0</u>	<u>38.8</u>							<u>WATER DEPTH TIDE 2.8'</u>			
<u>1</u>		<u>38.8</u>		<u>38.8</u>	<u>40.8</u>	<u>38.8</u>	<u>40.8</u>	<u>DRIVE SAMPLER JAR</u>		<u>GRAY SAND WITH CLAY PARTICLES</u>			
										<u>WEIGHT OF RODS AND HAMMER</u>			
										<u>PUSHED TO 40.8'</u>			
				<u>45.0</u>	<u>40.8</u>	<u>45.0</u>	-	<u>FISHTAIL</u>		<u>WASHED</u>			
<u>2</u>		<u>45.0</u>		<u>45.0</u>	<u>45.5</u>	<u>45.0</u>	<u>47.0</u>	<u>DRIVE SAMPLER JAR</u>		<u>GRAY SAND WITH TRACE CLAY, FIRM</u>			
				<u>45.5</u>	<u>46.0</u>					<u>11 BLOWS</u>			
				<u>46.0</u>	<u>46.5</u>					<u>10 BLOWS</u>			
				<u>46.5</u>	<u>47.0</u>								
				<u>51.0</u>	<u>47.0</u>	<u>51.0</u>	-	<u>FISHTAIL</u>		<u>WASHED</u>			
<u>3</u>		<u>51.0</u>		<u>51.0</u>	<u>51.5</u>	<u>51.0</u>	<u>53.0</u>	<u>DRIVE SAMPLER JAR</u>		<u>BROWN SAND WITH SHELL, VERY DENSE</u>			
				<u>51.5</u>	<u>52.0</u>					<u>23 BLOWS</u>			
				<u>52.0</u>	<u>52.5</u>					<u>81 BLOWS</u>			
				<u>52.5</u>	<u>53.0</u>								
										<u>TOTAL DEPTH 53.0'</u>			
NO. WATER TABLE/AT _____													
WEIGHT OF HAMMER <u>140 #</u>													
DROP DISTANCE <u>30"</u>													
DRIVE SAMPLER <u>2" x 1 1/8" x 24"</u>													
WES Form No. 819 April 1964										Sheet <u>1</u> of <u>1</u> Sheets			

SWF FORM 201
 12 July 1971
 PROJECT: Port Aransas-Corpus Christi Waterway
 LOCATION: Inner Basin
 GDLR NO. 1381
 BORING NO. 3ST-136
 TEST DATA SUMMARY
 DATE COMPLETED Oct. 1, 1971

FIELD NO.	Sample Depth, Feet	CLASSIFICATION	ELEVATION TOP BORING	SYMBOL	CONSISTENCY	POCKET (1) PENETROMETER	STAN. PENET. BLOWS (FT. (2))	MOISTURE CONTENT %	DRY DENSITY p. c. f.	L. L.	P. L.	Lab Sample No.	SIEVE ANALYSIS								
													PERCENT			INIT. WT.	ACC. WT. RTND. SIEVE NO. (3)				
													GRVL	SAND	FINES		NO. 4	NO. 10	NO. 40	NO. 200	
<u>1-J</u>	<u>38.8-40.8</u>	<u>Gray Sandy Clay</u>	<u>38.8-45'</u>	<u>CL</u>		<u>26</u>						<u>2425</u>									
<u>2-J</u>	<u>45-47</u>	<u>Gray Silty Sand</u>	<u>45'-53'</u>	<u>SM</u>	<u>0</u>	<u>21</u>	<u>27</u>					<u>2426</u>	<u>0</u>	<u>0</u>	<u>61</u>	<u>36</u>	<u>50</u>	<u>0</u>	<u>0</u>	<u>0</u>	<u>32</u>
<u>3-J</u>	<u>51-53</u>	<u>Shell fragments</u>	<u>51'-53'</u>		<u>VD</u>	<u>104</u>	<u>20</u>					<u>2427</u>	<u>0</u>	<u>2</u>	<u>66</u>	<u>32</u>	<u>50</u>	<u>1</u>	<u>3</u>	<u>7</u>	<u>32</u>

KEY: CONSISTENCY - CORRELATIVE SOILS (1) 1/2 in. Dia. Unconfined Compressive Strength
 VS Very Soft S Soft M Medium Stiff H Hard VL Very Loose L Loose ML Medium Dense VD Very Dense
 Bottomed at 53' Water at +38.8' Tide Reading 2.8'
 BORING NO. 3ST-136
 Sheet 1 of sheets 1